Two Inverse Problems Arising in Medical Imaging

Yifan Chang

A dissertation
submitted in partial fulfillment of the
requirements for the degree of

Doctor of Philosophy

University of Washington

2018

Reading Committee:

Gunther Uhlmann, Chair

Hart Smith

Yu Yuan

Program Authorized to Offer Degree:
Department of Mathematics

University of Washington

Abstract

Two Inverse Problems Arising in Medical Imaging

Yifan Chang

Chair of the Supervisory Committee:
Professor Gunther Uhlmann
Department of Mathematics

In this thesis, we discuss two inverse problems arising in medical imaging.

The first problem is about a hybrid imaging method using coupled boundary measurements, which combines electrical impedance tomography (EIT) with heat conduction. We prove uniqueness for this method in the two dimensional case, i.e. it uniquely determines the anisotropic electrical conductivity, the anisotropic thermal conductivity, and the product of heat capacity and heat density within a bounded domain in the plane up to a boundary-fixing diffeomorphism.

The second problem arises in positron emission tomography (PET), a medical imaging technique that aims to determine the distribution of radioactive tracers in a patient's body. The PET data needs some attenuation correction before it can be used to reconstruct the distribution, and the correction is usually achieved using attenuation coefficients reconstructed from another computed tomography (CT) scan. We show that the PET data is enough to recover certain types of singularities of the distribution (like jump discontinuities), which is usually enough for medical purpose, and thus that the extra CT scan is unnecessary.

TABLE OF CONTENTS

LIST OF FIGURES

GLOSSARY

EIT: Electrical impedance tomography

PET: Positron emission tomography

CT: Computerized tomography

CGO solution: Complex geometric optic solution

DtN map: Dirichlet-to-Neumann map

ACKNOWLEDGMENTS

First and foremost, I want to express my sincere thanks from the bottom of my heart to my advisor, Professor Gunther Uhlmann, for his kindness, intellectual guidance and encouragement throughout my Ph.D. years. I always feel so lucky and blessed to have such a great mathematician and more importantly, such a wonderful person as my mentor. Coming to the University of Washington and study with you is one of the best things that ever happened to me. My gratitude goes beyond these words.

I also want to thank Professors Hart Smith, Yu Yuan and Fang Han for serving as my committee.

The past ten years with mathematics have been amazing, I am able to get a glimpse of so many beautiful scenes, better than any other things in the world. Though I need to stop for the moment, I will always be grateful for this incredible journey. All of these could not happen without the help of two of my teachers, Ms Jing Fang and Mr Min Cheng. Also thanks to Tong Qin who set me up with the inverse problem summer school in 2013 which led my path to the University of Washington later.

The life towards a Ph.D. can be harsh sometimes and I can not make it without all my friends from different life periods. Many thanks to Changjing Wu, Yuan Li, Fang Han, Wenfang Xu, Yinsi Qi, Fei Liu, Junyang Qian, Hongliang Lu, Wen Yang, Zichun Ye, Jiaxing Wang, Ting Zhou, Yang Yang, Ru-yu Lai, Hanming Zhou, Yue Zhao, Daiwei He, Zijian Li, Yunhao Shen, Yunxiang Zhang, Shen Ren, etc. Special thanks to my girlfriend Yi Li for staying with me after so many years.

Finally I want to thank my loving parents for your unconditional love and support.

DEDICATION

to my family

Chapter 1

INTRODUCTION

Over the past several decades, medical imaging techniques have revolutionized health care. Imaging modalities, such as computed tomography (CT) scan, ultrasound, magnetic resonance imaging (MRI), provide noninvasive ways to reconstruct internal physical properties like electrical conductivities, attenuation coefficients, etc. The reconstructed physical properties reveal the internal structure of patient's body, since different tissues may differ a lot in these properties, and are usually presented to doctors in form of 2D/3D images. These techniques are vital in disease diagnosis/early detection, surgery and treatment, and have fundamentally altered the practice of medicine. Any improvements in image accuracy, contrast or resolution can have a positive impact on thousands of patients.

While imaging modalities differ in the underlining physical processes, device and hardware, data acquisition and signal processing, etc., at the core of each modality, there is an inverse problem that first establishes an appropriate mathematical model, based on the physical principles the modality operates on, to interpret the measurements and then tries to find an inversion formula/a numerical algorithm that reconstructs the desired physical properties from the measured data. Mathematically, an inverse problem is usually formulated as follows: let X be the space of functions $f : \Omega \to \mathbf{R}^m$ where $\Omega \subset \mathbf{R}^n$, $A : X \to Y$ be an operator from the function space X to some data space Y, given $d = Af + \epsilon$ where ϵ is some random noise in data space Y, the inverse problem aims to recover f from d. In medical imaging context, f represents the physical properties we want to recover and m might be greater than 1 which corresponding to multiple properties or some property with vector/matrix representation. Ω represents patient's body ($n = 3$) or a 2D body slice ($n = 2$). A corresponds to the imaging process, ϵ is the random noise due to various reasons like precision limitation of the device

which is inevitable in practice and d represents the measured data we have.

For an inverse problem, usually we need to understand the following:

- Uniqueness: in the noise free case, does the measured data uniquely determine the desired properties? That is, does $Af_1 = Af_2$ imply $f_1 = f_2$?

- Existence/Range characterization: for a given element in the data space Y, is there a $f \in X$ such that $Af = d$? That is, what is the range of the operator A? Knowing the range also helps when given a noisy data, we may want to first project it into the range.

- Inversion formula: when existence and uniqueness are guaranteed, the problem is invertible, then can we find some explicit formula that reconstructs f from d? If so, is there an efficient numerical algorithm to implement it?

- Stability: when the problem is invertible, how sensitive is it to the measured data? Can a small change in measurements lead to a huge difference in the reconstructions? Unfortunately, inverse problems are often highly unstable.

- Gaps between continuous and discrete: most of the models we establish are continuous, which work well for theoretical analysis, while in reality, all computations are discrete. How should we connect the continuous results with discrete computation? For example, the wavefront set we are going to use later in this thesis is great for theoretical analysis, but how to use it for discrete computations is still not well understood.

See [46], [18], [40] for more information about mathematical inverse problems in medical imaging.

We discuss two inverse problems arising in medical imaging in this thesis. In Chapter 2, we consider uniqueness for a hybrid imaging method which combines electrical impedance tomography (EIT) with heat conduction. Originally proposed in [33], this method uses

coupled boundary measurements to determine both electrical and heat transfer properties within some bounded domain. Uniqueness was proven in [33] for isotropic properties in three dimension or higher. We consider anisotropic properties within a bounded plane domain and prove that the method uniquely determines the properties up to a boundary-fixing diffeomorphism. In Chapter 3, we consider an inverse problem arising in positron emission tomography (PET). PET is a functional imaging modality that is used to observe metabolic processes in the body. Before the PET scan, patients are injected with some radioactive tracers; the goal is to recover the distribution of the tracers by counting the number of simultaneously-detected photon pairs (which are generated when the tracers decay) along each line. These counts need some correction due to body attenuation before they can be used to reconstruct the distribution. The correction is usually achieved using the body's attenuation coefficient which is obtained by another CT scan. In medical imaging, it is usually the singularities rather than the exact values of the reconstructed functions that provide useful information: for example jump discontinuities usually correspond to boundaries of different tissues. We show that if we only want to recover certain types of singularities (like jump discontinuities) of the target functions, the attenuation correction based on the extra CT scan is actually not needed: most of this information is contained in the PET data.

Chapter 2

UNIQUENESS FOR THE EIT/HEAT SYSTEM

2.1 Problem set up

In spite of the great success various medical imaging modalities have achieved, each stand-alone method usually has its drawback limited by the underlining physical process. For example, thanks to efficient reconstruction algorithm and data redundancy, CT image usually exhibits high resolution but low contrast since the attenuation coefficients, the physical properties CT scan reconstruct, for healthy and unhealthy tissues are not that different, which can make diagnose pretty difficult. While at the same time, optical tomography usually exhibits low resolution but high contrast. This suggests us to use coupled imaging modalities to combine advantages and overcome drawbacks. These hybrid imaging methods have been more and more popular in recent years. Successful examples include photo-acoustic tomography, thermo-acoustic tomography, see [5], [34], [39], [59], [51], [13] for more discussions.

In [33], the authors proposed a new hybrid imaging method that combines EIT with heat conduction. They proved that the method uniquely determined isotropic electrical and heat transfer properties within some bounded domain in $\mathbf{R}^n$ for $n \geq 3$, by using coupled boundary measurements. In this chapter, we prove that in the two dimensional case, the method uniquely determines anisotropic properties up to a boundary-fixing diffeomorphism.

Now we set up the problem as follows, given a bounded domain $\Omega \subset \mathbf{R}^2$ with smooth boundary (for the purpose of this thesis, we just formulate the problem for plane domains, but the set up is the same for $n > 2$), we consider two physical processes. First, we put a time-dependent voltage distribution $f(\boldsymbol{x}, t) \in C(\mathbf{R}_+, H^{\frac{1}{2}}(\partial\Omega))$ at the boundary $\partial\Omega$, and assuming there are no sinks or sources inside Ω. Then the resulting voltage distribution

$u(\boldsymbol{x},t)$ throughout the whole domain is governed by the conductivity equation

$$\nabla\cdot(\boldsymbol{\gamma}(\boldsymbol{x})\nabla u(\boldsymbol{x},t))=0,\quad \boldsymbol{x}\in\Omega \qquad \text{and} \quad u|_{\partial\Omega}=f, \tag{2.1}$$

where ∇ is the standard gradient operator, $\nabla\cdot$ is the standard divergence operator and $\boldsymbol{\gamma}(\boldsymbol{x})$ is the electrical conductivity of Ω, the first unknown property of the domain that we want to determine. Instead of only considering isotropic electrical conductivities like [33] did, we also include anisotropic conductivities, i.e. $\boldsymbol{\gamma}(\boldsymbol{x})$ is a positive definite matrix at each point, and we assume it is bounded below, i.e. $\exists c>0$ s.t. $||\boldsymbol{\gamma}(\boldsymbol{x})||_2>c$ where $||\cdot||_2$ is the induced matrix 2-norm defind by $||\boldsymbol{A}||_2\triangleq \sup_{\boldsymbol{x}\in\mathbf{R}^n}\frac{||\boldsymbol{A}\boldsymbol{x}||_2}{||\boldsymbol{x}||_2}$ where $||\cdot||_2$ is just the usual vector 2-norm. Then $u(\boldsymbol{x},t)\in C(\mathbf{R}_+,H^1(\Omega))$ since for any fixed time t, equation (2.1) is a second order elliptic equation and the standard existence theory assures us that there exists a unique solution $u(\cdot,t)\in H^1(\Omega)$. Also we remark here that the boundary condition makes sense since we can extend the usual restriction operator $R: C^\infty(\bar{\Omega})\to C^\infty(\partial\Omega)$ to a bounded operator from $H^1(\Omega)$ to $H^{\frac{1}{2}}(\partial\Omega)$.

The second process is heat transfer. It is known that electrical current generates heat which diffuses throughout the domain. We model this by considering the temperature distribution $\psi(\boldsymbol{x},t)$, which is governed by the heat equation

$$\kappa^{-1}(\boldsymbol{x})\partial_t\psi(\boldsymbol{x},t)=\nabla\cdot(\boldsymbol{A}(\boldsymbol{x})\nabla\psi(\boldsymbol{x},t))+S(\boldsymbol{x},t),\quad \boldsymbol{x}\in\Omega \quad\text{and}\quad t\geq 0, \tag{2.2}$$

$$\psi(\boldsymbol{x},0)=0,\quad \forall\boldsymbol{x}\in\Omega \quad \psi(\boldsymbol{x},t)=0,\quad \forall\boldsymbol{x}\in\partial\Omega \quad\text{and}\quad t\geq 0, \tag{2.3}$$

where $\kappa(\boldsymbol{x})=c(\boldsymbol{x})^{-1}\rho(\boldsymbol{x})^{-1}$ is the reciprocal of the product of the heat capacity $c(\boldsymbol{x})$ and density $\rho(\boldsymbol{x})$, $\boldsymbol{A}(\boldsymbol{x})$ is the thermal conductivity and is represented by a positive definite matrix at each point. We also want to determine κ and $\boldsymbol{A}$ and assume they are also bounded below thoughtout the domain. The term $S(\boldsymbol{x},t)$, which is called the energy density of the electrical field, is defined by $S(\boldsymbol{x},t)=\nabla u(\boldsymbol{x},t)\cdot\boldsymbol{\gamma}(\boldsymbol{x})\nabla u(\boldsymbol{x},t)$, where $u(\boldsymbol{x},t)$ is the solution to (2.1) and $S(\boldsymbol{x},t)$ will act as a source term in the heat equation. The initial and boundary condition (2.3) means that the temperature (after some shift) throughout the domain equal 0 when $t=0$ and the boundary temperature is kept at 0 for all $t\geq 0$. As [33] did, we also

assume that the heat transfer is sufficiently slow so that the quasistatic model (2.1) for the voltage $u(\boldsymbol{x})$ is still realistic.

Define coupled boundary measurements, namely the voltage-to-heat flow map $\Sigma_{\boldsymbol{\gamma},\kappa,\boldsymbol{A}}$, as follows:

$$\Sigma_{\boldsymbol{\gamma},\kappa,\boldsymbol{A}}: \quad f(\boldsymbol{x},t) \quad \Rightarrow \quad \boldsymbol{\nu}\cdot\boldsymbol{A}\nabla\psi(\boldsymbol{x},t), \quad \boldsymbol{x}\in\partial\Omega, \tag{2.4}$$

where $\boldsymbol{\nu}$ is the unit outer normal vector at the boundary. In other words, $\Sigma_{\boldsymbol{\gamma},\kappa,\boldsymbol{A}}$ maps a time-dependent electrical boundary voltage $f(\boldsymbol{x},t)$ to the outcoming heat flow $\boldsymbol{\nu}\cdot\boldsymbol{A}\nabla\psi(\boldsymbol{x},t)$. We study with what information about the internal properties $\boldsymbol{\gamma}$, κ and $\boldsymbol{A}$ can we recover from the boundary measurement $\Sigma_{\boldsymbol{\gamma},\kappa,\boldsymbol{A}}$.

The first part of the method is related to EIT, which is also known as Calderón's inverse problem, where one tries to determine bodies' internal electrical conductivities by using voltage-to-current measurements at the boundary. It has been intensively studied over the past few decades and we will review some basic results below.

As mentioned above, unlike [33] where the authors only consider isotropic electrical conductivities and show that $\Sigma_{\gamma,\kappa,\boldsymbol{A}}$ determines γ, κ and $\boldsymbol{A}$ uniquely, we also consider anisotropic electrical conductivities. As we know for the anisotropic EIT/Calderón's inverse problem, given any boundary-fixing diffeomorphism $\boldsymbol{F}$ of Ω, we define the pushforward of $\boldsymbol{\gamma}$ by $\boldsymbol{F}$ as $\boldsymbol{F}_*\boldsymbol{\gamma}(\boldsymbol{x}) = \frac{D\boldsymbol{F}\boldsymbol{\gamma}D\boldsymbol{F}^T}{|D\boldsymbol{F}|}\circ\boldsymbol{F}^{-1}(\boldsymbol{x})$, where DF is the Jacobian matrix of F, then it can be proved that $\Lambda_{\boldsymbol{F}_*\boldsymbol{\gamma}} = \Lambda_{\boldsymbol{\gamma}}$, where $\Lambda_{\boldsymbol{\gamma}}$ is the boundary voltage-to-current measurements, or mathematically the standard Dirichlet-to-Neumann (DtN) map that maps static boundary voltage (the Dirichlet boundary data, i.e. the boundary value) to the outcoming current (the Neumann boundary data, i.e. the outer normal derivative). It means that any conductivity and its pushforward have the same measured data, or in other words, the DtN map can not tell conductivity and its pushforward apart. The reason for that is conductivity equation is independent of the choice of coordinates and the whole pushforward can be seen as change of coordinates within the domain. For the two dimensional case, it has been proved that change of coordinates is the only obstacle to uniqueness, i.e. if $\Lambda_{\boldsymbol{\gamma}_1} = \Lambda_{\boldsymbol{\gamma}_2}$, then $\boldsymbol{\gamma}_2$ is the pushforward of $\boldsymbol{\gamma}_1$ by some boundary-fixing diffeomorphism $\boldsymbol{F}$. Similarly we can apply the same change of

coordinates to the heat equation, so for the two dimensional case if we consider anisotropic electrical conductivities, the best uniqueness result for this hybrid modality is that $\Sigma_{\boldsymbol{\gamma},\kappa,\boldsymbol{A}}$ determines $\boldsymbol{\gamma}, \kappa, \boldsymbol{A}$ uniquely up to a boundary-fixing diffeomorphism. We prove that this is indeed the case and have the following result.

Theorem 1 (Chang). *Assume $\Omega \subset \mathbf{R}^2$ is a bounded domain with smooth boundary, $\kappa_i(\boldsymbol{x}) \in C^\infty(\bar{\Omega})$, $\boldsymbol{\gamma}_i(\boldsymbol{x})$, $\boldsymbol{A}_i(\boldsymbol{x}) \in C^\infty(\bar{\Omega}, \mathcal{S}^2_{++})$, where $\mathcal{S}^2_{++}$ stands for 2×2 positive definite matrices and κ_i, $||\boldsymbol{\gamma}_i(\boldsymbol{x})||_2$, $||\boldsymbol{A}_i(\boldsymbol{x})||_2$ are bounded below by a positive number, $i = 1, 2$. If $\Sigma_{\boldsymbol{\gamma}_1,\kappa_1,\boldsymbol{A}_1} = \Sigma_{\boldsymbol{\gamma}_2,\kappa_2,\boldsymbol{A}_2}$, then there exists a diffeomorphism $\boldsymbol{F} : \bar{\Omega} \to \bar{\Omega}$, which fixes the boundary, i.e. $\boldsymbol{F}|_{\partial\Omega} = id$, such that $\kappa_2(\boldsymbol{x}) = \kappa_1 |D\boldsymbol{F}| \circ \boldsymbol{F}^{-1}(\boldsymbol{x})$, $\boldsymbol{\gamma}_2(\boldsymbol{x}) = \frac{D\boldsymbol{F}\boldsymbol{\gamma}_1 D\boldsymbol{F}^T}{|D\boldsymbol{F}|} \circ \boldsymbol{F}^{-1}(\boldsymbol{x})$ and $\boldsymbol{A}_2(\boldsymbol{x}) = \frac{D\boldsymbol{F}\boldsymbol{A}_1 D\boldsymbol{F}^T}{|D\boldsymbol{F}|} \circ \boldsymbol{F}^{-1}(\boldsymbol{x})$, where $(D\boldsymbol{F})_{ij} = \frac{\partial F_i}{\partial x_j}$ is the Jacobian matrix of $\boldsymbol{F}$.*

The rest of this chapter is organized as follows. We first review some basic results about EIT/Calderón's inverse problem in Section 2.2. In Section 2.3 we explain the outline of the proof. In Section 2.4 we do a brief review of the nonuniqueness caused by the change of coordinates. In Section 2.5, we show that the conductivity is determined uniquely up to a boundary-fixing diffeomorphism. An important density argument is proved in Section 2.6 and is later used in Section 2.7 to determine the heat properties up to the same diffeomorphism arises in Section 2.5.

Remark 1. *The regularity assumption in the theorem may not be optimal and may be improved by a more refined analysis. From now on, we will just assume everything is smooth without further mentioning.*

2.2 Review of EIT

EIT, or more generally known as Calderón's inverse problem aims to determine the electrical conductivity of some medium by making boundary voltage-to-current measurements. The problem is formulated as follows, Ω is a bounded domain in $\mathbf{R}^n$, $n \geq 2$, when imposed with a static boundary voltage f, the voltage u throughout the domain, by Ohm's law, satisfies

the conductivity equation,

$$\nabla \cdot (\boldsymbol{\gamma}(\boldsymbol{x})\nabla u(\boldsymbol{x})) = 0, \quad \boldsymbol{x} \in \Omega \qquad \text{and} \quad u|_{\partial\Omega} = f, \tag{2.5}$$

where $\boldsymbol{\gamma}(\boldsymbol{x})$ represents the electrical conductivity at each point (a scalar if the conductivity is isotropic and a positive definite matrix if the conductivity is anisotropic) and we assume it is bounded below. (2.5) is an elliptic partial differential equation and by the standard existence theory, for any boundary voltage $f \in H^{\frac{1}{2}}(\partial\Omega)$, we have a unique solution $u \in H^1(\Omega)$. Then as mentioned above, we measure the outcoming current at the boundary i.e. $\boldsymbol{\nu} \cdot \boldsymbol{\gamma}\nabla u|_{\partial\Omega}$, where $\boldsymbol{\nu}$ is the unit outer normal vector. This defines the voltage-to-current map, or the DtN map induced by $\boldsymbol{\gamma}$ that maps any boundary voltage to the current flux at the boundary:

$$\Lambda_{\boldsymbol{\gamma}} : \quad f \quad \Longrightarrow \quad \boldsymbol{\nu} \cdot \boldsymbol{\gamma}\nabla u|_{\partial\Omega}. \tag{2.6}$$

The Calderón's inverse problem is can we determine $\boldsymbol{\gamma}$ from $\Lambda_{\boldsymbol{\gamma}}$.

The problem was proposed by Dr. Alberto Calderón who first came across it while working as an engineer for some oil company in the 1950's and published his result [10] in 1980. Ever since then, it has been intensively studied and applied to different industries as well. Theoretically, there have been many results on uniqueness ([10], [32], [64], [65], [35], [25], [24], [12], [43], [2]), stability ([1]), reconstruction and the corresponding numerical methods ([42], [41], [57], [6]). See [69], [70] for general reviews. For applications, besides in medical imaging where it has been wildly used for detecting pulmonary emboli (see [14] for more information), it has also been applied to areas like geophysical prospection, Schlumberger-Doll company was founded to find oil by using electromagnetic methods.

For the sake of this thesis, we briefly review some uniqueness results for EIT/Calderón's inverse problem. For isotropic conductivities, A. Caldorón [10] showed that the linearization of the map $\Phi : \gamma \to \Lambda_\gamma$ was injective in 1980. R. Kohn and M. Vogelius [32] showed that given a domain with smooth boundary, if $\gamma(x)$ was smooth near $\partial\Omega$, then γ and all its normal derivatives were uniquely determined by Λ_γ. J. Lee and G. Uhlmann [35] proved the same result using the idea that Λ_γ was actually a pseudodifferential operator of order

1 on $\partial\Omega$ and boundary values and normal derivatives of γ were related to the symbol of Λ_γ. Then if the conductivity was analytic, we could reconstruct it through Λ_γ. The first global uniqueness result was proven by J. Sylvester and G. Uhlmann [64] in 1987 for smooth conductivity within a domain with smooth boundary in dimension three or higher. Since then the regularity assumption on conductivity and domain boundary were relaxed by several authors based on similar approach, see [47], [8]. Inspired by the work of B. Haberman and D. Tataru [25], [24], P. Caro and K. M. Rogers [12] proved the uniqueness result for $n \geq 3$, Lipschitz conductivity which was bounded below within a domain with Lipschitz boundary. For the two dimensional case, the approach usually involved complex analysis by the nature of the dimension and was always handled separately. Some early results include R. Kohn and M. Vogelius [32], Z. Sun and G. Uhlmann [60]. In 1995, Nachman [43] gave a uniqueness result for conductivity with two derivatives. The regularity assumption was relaxed to $W^{1,p}$ conductivity with $p > 2$ by R. Brown and G. Uhlmann [7], then to L^∞ conductivity bounded from above and blow by the work of K. Astala and L. Päivärinta [2].

For anisotropic conductivities, as mentioned above, Λ_γ is not able to tell a conductivity with its pushforward by any boundary-fixing diffeomorphism apart. Then we wonder does $\Lambda_{\boldsymbol{\gamma}_1} = \Lambda_{\boldsymbol{\gamma}_2}$ implies $\boldsymbol{\gamma}_2$ is the pushforward of $\boldsymbol{\gamma}_1$ by some boundary-fixing diffeomorphism. For the two dimensional case, the statement is true and was proved by J. Sylvester [62] for conductivity close to constant, Z. Sun, G. Uhlmann [61] for $W^{1,p}$ conductivity and finally K. Astala, M. Lassas and L. Päivärinta [3] for L^∞ conductivity. The idea is to convert the anisotropic problem into an equivalent isotropic case and the method only works for two dimension since it relies heavily on complex analysis. For dimension three and higher, the problem is still largely open. D. Ferreira, C. Kenig, M. Salo, and G. Uhlmann [21] prove it under certain additional assumptions by using limiting Carleman weight and geodesic ray transform.

Next we state some facts that are important in the proofs of these uniqueness results. First, when the conductivity is isotropic, (2.1) is closely related to a Schrödinger equation through the so called Liouville transform: assume $0 < \gamma(\boldsymbol{x}) \in C^2(\bar{\Omega})$ and $u(\boldsymbol{x}) \in H^1(\Omega)$

solves the conductivity equation (2.5) with boundary value $u|_{\partial\Omega} = f \in H^{\frac{1}{2}}(\partial\Omega)$, define u_S, q, g as follows,

$$u_S(\boldsymbol{x}) = \gamma^{\frac{1}{2}} u, \quad q = \frac{\Delta\gamma^{\frac{1}{2}}}{\gamma^{\frac{1}{2}}}, \quad g = \gamma^{\frac{1}{2}} f, \tag{2.7}$$

then it can be proved that they solve the following Schrödinger equation

$$(-\Delta + q(\boldsymbol{x}))u_S(\boldsymbol{x}) = 0, \quad \boldsymbol{x} \in \Omega \qquad \text{and} \quad u_S|_{\partial\Omega} = g. \tag{2.8}$$

Notice that (2.8) is uniquely solvable for any given boundary data $g \in H^{\frac{1}{2}}(\partial\Omega)$ when 0 is not a Dirichlet eigenvalue of $-\Delta + q(\boldsymbol{x})$, which is always satisfied if $q(x)$ is derived from some conductivity γ as above. Then we can similarly define the DtN map for the potential q that maps the boundary value to the outer normal derivative,

$$\Lambda_q : \quad g \quad \Longrightarrow \quad \boldsymbol{\nu} \cdot \nabla v|_{\partial\Omega}, \tag{2.9}$$

and another inverse problem arises naturally that whether Λ_q uniquely determines q or not. Also based on the above derivation, the relation between Λ_γ and Λ_q is given by:

$$\Lambda_q f = \gamma^{\frac{1}{2}} \Lambda_\gamma \gamma^{-\frac{1}{2}} f + \frac{1}{2}\gamma^{-1}\partial_{\boldsymbol{n}}\gamma f, \quad \forall f \in C^\infty(\partial\Omega). \tag{2.10}$$

Both Λ_γ and Λ_q maps from $H^{\frac{1}{2}}(\partial\Omega)$ to $H^{-\frac{1}{2}}(\partial\Omega)$, which is the dual space of $H^{\frac{1}{2}}(\partial\Omega)$. For example,

$$\forall f, g \in H^{\frac{1}{2}}(\partial\Omega), \quad < \Lambda_{\boldsymbol{\gamma}} f, g >= \int_\Omega \nabla u_f \cdot (\boldsymbol{\gamma}\nabla v_g) d\boldsymbol{x}, \tag{2.11}$$

where u_f is the solution to (2.5) with boundary value f, v_g is any function in $H^1(\Omega)$ such that $v_g|_{\partial\Omega} = g$ and $< \cdot, \cdot >$ is the usual duality pair between $H^{-\frac{1}{2}}(\Omega)$ and $H^{\frac{1}{2}}(\partial\Omega)$. It is easy to see that (2.11) does not depend on the choice of v_g as long as $v_g|_{\partial\Omega} = g$, then we may take v_g to be the unique solution to (2.5) with boundary value g, plus the fact that γ is symmetric, we have

$$< \Lambda_{\boldsymbol{\gamma}} f, g >= \int_\Omega \nabla u_f \cdot (\boldsymbol{\gamma}\nabla v_g) d\boldsymbol{x} = \int_\Omega \nabla v_g \cdot (\boldsymbol{\gamma}\nabla u_f) d\boldsymbol{x} =< \Lambda_{\boldsymbol{\gamma}} g, f >$$

Similarly, Λ_q satisfies

$$< \Lambda_q f, g >= \int_\Omega \nabla u_f \cdot \nabla v_g + q u_f v_g d\boldsymbol{x} =< \Lambda_q g, f >,$$

here u_f and v_g are solutions to (2.5) and (2.8) with boundary values f and g. Then if $\Lambda_{\gamma_1} = \Lambda_{\gamma_2}$, we have

$$\forall f, g \in H^{\frac{1}{2}}(\partial\Omega), < \Lambda_{\gamma_1} f, g >=< \Lambda_{\gamma_2} f, g >=< \Lambda_{\gamma_2} g, f > .$$

Let u_f be the unique solution to (2.5) with boundary value f and conductivity γ_1, v_g be the unique solution to (2.5) with boundary value g and conductivity γ_2, using the above properties,

$$\int_\Omega (\nabla u_f)^T \cdot (\boldsymbol{\gamma_1} \cdot \nabla v_g) d\boldsymbol{x} =< \Lambda_{\gamma_1} f, g >=< \Lambda_{\gamma_2} g, f >= \int_\Omega (\nabla u_f)^T \cdot (\boldsymbol{\gamma_2} \cdot \nabla v_g) d\boldsymbol{x},$$

which implies

$$\int_\Omega (\nabla u_f)^T \cdot (\boldsymbol{\gamma_1} - \boldsymbol{\gamma_2}) \cdot \nabla v_g d\boldsymbol{x} = 0.$$

So for isotropic γ_1, γ_2, uniqueness can be proved by showing the space spanned by $(\nabla u_f)^T \cdot \nabla v_g$, where u_f and v_g are arbitrary solutions to (2.5) with conductivities γ_1 and γ_2, is dense in $L^2(\Omega)$. Another approach for isotropic conductivities is as follows, from the boundary determination result [32], $\Lambda_{\gamma_1} = \Lambda_{\gamma_2}$ implies

$$\gamma_1|_{\partial\Omega} = \gamma_2|_{\partial\Omega}, \quad \partial^n_{\boldsymbol{\nu}} \gamma_1 = \partial^n_{\boldsymbol{\nu}} \gamma_2 \tag{2.12}$$

Consider the corresponding Schrödinger equations obtained by the Liouville transform, we have $\Lambda_{q_1} = \Lambda_{q_2}$ based on (2.10) and (2.12). Using similar derivation as above, this further implies

$$\int_\Omega (q_1 - q_2) u_f v_g d\boldsymbol{x} = 0,$$

where u_f, v_g are solutions to (2.8) with boundary values f and g. Then we can prove $q_1 = q_2$ by showing the space spanned by $u_f v_g$ are dense in $L^2(\Omega)$, which further implies $\gamma_1 = \gamma_2$. The density is usually proved by constructing enough solutions, the most important and successful example is the Complex Geometric Optics (CGO) solutions constructed by J. Sylvester and G. Uhlmann [64] among which for any $\boldsymbol{\xi}$, we can find pairs of solutions whose products converge to $e^{i\boldsymbol{x}\cdot\boldsymbol{\xi}}$.

2.3 Outline of the proof

In this section, we give the outline of the proof for Theorem 1.

1. First, we recover the quadratic forms $Q_{\boldsymbol{\gamma}_i}$ induced by $\boldsymbol{\gamma}_i$, which will be defined later, from the voltage-to-heat flow map $\Sigma_{\boldsymbol{\gamma}_i,\kappa_i,\boldsymbol{A}_i}$. $Q_{\boldsymbol{\gamma}_i}$ contains the same information as the DtN map $\Lambda_{\boldsymbol{\gamma}_i}$ does. The reconstruction is done by taking special input data (static ones). The main idea behind this is that the quadratic form maps any static boundary voltage to the amount of energy needed to maintain that due to the energy loss caused by the heat generated by the current. So in the static case, this energy should be equal to the heat flow coming out due to the conservation of energy. Then based on the exiting result for the two dimensional Calderón's inverse problem, we prove that the two conductivities are the same up to certain boundary-fixing diffeomorphism, i.e. one is the pushforward of the other.

2. The conductivity equation (2.1) and the heat equation (2.2) are related through the electrical energy density $S(\boldsymbol{x},t) = \nabla u(\boldsymbol{x},t)\cdot\boldsymbol{\gamma}(\boldsymbol{x})\nabla u(\boldsymbol{x},t)$, which is the outcome of (2.1) and acts as an input of (2.2). Now we take spacial input data f which is separated in $\boldsymbol{x}$ and t, i.e. $f(\boldsymbol{x},t) = h(\boldsymbol{x})g(t)$, then the corresponding solutions to (2.1) will have the form $u(\boldsymbol{x},t) = u_0(\boldsymbol{x})g(t)$, where u_0 is the static solutions to (2.5) with boundary value $h(\boldsymbol{x})$, and $S(\boldsymbol{x},t) = (\nabla u_0(\boldsymbol{x})\cdot\boldsymbol{\gamma}(\boldsymbol{x})\nabla u_0(\boldsymbol{x}))g(t)$. Next we show the space spanned by $\{\nabla u_0\cdot\boldsymbol{\gamma}\nabla u_0\}$ is actually dense in $L^2(\Omega)$. So we can conclude that the voltage-to-heat flow map $\Sigma_{\boldsymbol{\gamma},\kappa,\boldsymbol{A}}$ contains information for putting arbitrary variable-separated source $S(\boldsymbol{x},t) = w(\boldsymbol{x})g(t)$ into (2.2) by the continuous dependence of the solution to (2.2) on $S(\boldsymbol{x},t)$. The most important part in this step, which is also the core of this chapter, is to prove the density argument and it is obtained by using special solutions to the Schrödinger equation related with (2.5), including the CGO solutions and the solutions constructed by A. Bukhgeim in [9].

3. Based on the fact in the second step and a change of coordinates (arising from the

first step), the problem has become that if for any variable-separated source $S(\boldsymbol{x},t) = w(\boldsymbol{x})g(t)$, the out-coming heat flows are the same for two systems, then their heat properties must coincide. This has already been proven in [33]. The basic idea is once again to take special input data (pulse sources which converge to $w(\boldsymbol{x})\delta(t)$) and solve the heat equations using eigenfunctions of the operator $\kappa_i\nabla\cdot(\boldsymbol{A_i}(\boldsymbol{x})\nabla)$ in some weighted L^2 space. And with the help of some boundary determination results, it can be proved that all the eigenvalues and eigenfunctions of the two operator $\kappa_i\nabla\cdot(\boldsymbol{A_i}(\boldsymbol{x})\nabla)$ are the same, which leads to $\boldsymbol{A}_1 = \boldsymbol{A}_2$ then $\kappa_1 = \kappa_2$.

Remark 2. *Our proof for step one is slightly different with the one in [33] that emphasises more on the physical interpretation. The arguments in step three have already been proven in [33] for dimension $n \geq 2$, but their strategy to prove the density argument stated in step two can not work for the two dimensional case.*

2.4 Obstacle to uniqueness

In this section, we review some basic facts about the obstacle to uniqueness caused by change of coordinates or sometimes called gauge transformation induced by a boundary-fixing diffeomorphism of Ω. This nonuniqueness happens since physical principles do not depend on the choice of coordinates and what we see here is essentially describing the same physical phenomenon using different coordinate system. The results in this section are valid for dimension $n \geq 2$. They can actually be proved by some tedious direct calculations that only evolve basic calculus. But instead, we are going to prove them using Riemannian geometry which provides some new perspective and can further relate these problems with other geometric inverse problems (which is beyond the scope of this thesis). In this whole section, we assume that $\boldsymbol{F} : \bar{\Omega} \to \bar{\Omega}$ is a diffeomorphism of $\bar{\Omega}$, which is a at least C^2 and fixes the boundary, i.e. $\boldsymbol{F}|_{\partial\Omega} = id$. We first start with the conductivity equation (2.5) and have the following result.

Lemma 1. *If $u(\boldsymbol{x})$ is a solution to (2.5), then $\tilde{u}(\boldsymbol{x}) \triangleq u \circ \boldsymbol{F}^{-1}(\boldsymbol{x}) = u(\boldsymbol{F}^{-1}(\boldsymbol{x}))$ solves (2.5)*

with conductivity $\tilde{\boldsymbol{\gamma}} = \boldsymbol{F}_*\boldsymbol{\gamma} \triangleq \frac{D\boldsymbol{F}\boldsymbol{\gamma}D\boldsymbol{F}^T}{|D\boldsymbol{F}|} \circ \boldsymbol{F}^{-1}$*, which is sometimes called the pushforward of* $\boldsymbol{\gamma}$ *and* $(D\boldsymbol{F})_{ij} = \frac{\partial F_i}{\partial x_j}$ *is the Jacobian matrix of* $\boldsymbol{F}$ *as usual. As a result, we have* $\Lambda_{\boldsymbol{\gamma}} = \Lambda_{\boldsymbol{F}_*\boldsymbol{\gamma}}$.

As mentioned above, when $n \geq 3$, we are going to relate (2.5) with the Laplace-Beltrami operator $\Delta_{g_{\boldsymbol{\gamma}}}$ for some properly chosen metric $g_{\boldsymbol{\gamma}}$ associated with $\boldsymbol{\gamma}$

$$g_{\boldsymbol{\gamma}} \triangleq |\boldsymbol{\gamma}|^{\frac{1}{n-2}}\boldsymbol{\gamma}^{-1}, \tag{2.13}$$

then $\nabla\cdot(\boldsymbol{\gamma}(\boldsymbol{x})\nabla u(\boldsymbol{x})) = |g_{\boldsymbol{\gamma}}|^{\frac{1}{2}}\Delta_{g_{\boldsymbol{\gamma}}}u = 0$ means that u is a harmonic function on the Riemanian manifold $(\Omega, g_{\boldsymbol{\gamma}})$. Notice an important fact that

$$g_{\tilde{\boldsymbol{\gamma}}} = g_{\boldsymbol{F}_*\boldsymbol{\gamma}} = (\boldsymbol{F}^{-1})^* g_{\boldsymbol{\gamma}},$$

i.e. the metric corresponding to the push forward conductivity is just the pull back of the metric $g_{\boldsymbol{\gamma}}$ by $\boldsymbol{F}^{-1}$. Then since the Laplace-Beltrami operator is defined intrinsically, we have

$$0 = \Delta_{g_{\boldsymbol{\gamma}}}u = \Delta_{(\boldsymbol{F}^{-1})^* g_{\boldsymbol{\gamma}}}u \circ \boldsymbol{F}^{-1} = \Delta_{g_{\tilde{\boldsymbol{\gamma}}}}\tilde{u},$$

which implies that $\tilde{u}$ solves (2.1) with conductivity $\tilde{\boldsymbol{\gamma}}$. But we may have a problem when $n = 2$, since the metric $g_{\boldsymbol{\gamma}}$ in (2.13) will not be well defined. We will fix this problem later in the proof of Lemma 2. Another equivalent way to see this is using the fact that $u(\boldsymbol{x})$ solves (2.5) if and only if $u(\boldsymbol{x})$ is the unique global minimizer of the energy functional $E_{\boldsymbol{\gamma}}(u) = \int_\Omega \nabla u(\boldsymbol{x}) \cdot \boldsymbol{\gamma}(\boldsymbol{x})\nabla u(\boldsymbol{x})\, dx$ within the class of functions with boundary value f. An easy calculation using change of coordinates shows that $E_{\boldsymbol{\gamma}}(u(\boldsymbol{x})) = E_{\boldsymbol{F}_*\boldsymbol{\gamma}}(u \circ \boldsymbol{F}^{-1}(\boldsymbol{x}))$. So $u(\boldsymbol{x})$ minimizes $E_{\boldsymbol{\gamma}}(\cdot)$ is equivalent to $\tilde{u} = u \circ \boldsymbol{F}^{-1}$ minimizes $E_{\tilde{\boldsymbol{\gamma}}}(\cdot) = E_{\boldsymbol{F}_*\boldsymbol{\gamma}}(\cdot)$, which means $u \circ \boldsymbol{F}^{-1}$ solves (2.5) with conductivity $\boldsymbol{F}_*\boldsymbol{\gamma}$. To show that $\Lambda_{\boldsymbol{\gamma}} = \Lambda_{\boldsymbol{F}_*\boldsymbol{\gamma}}$, either use the Riemannian geometry approach which will be explained below, or just calculate directly and recall the fact that $\boldsymbol{F}$ is identity when restricted to the boundary.

Then we move on to the heat equation (2.2) and show the following result.

Lemma 2. *If* $\psi(\boldsymbol{x}, t)$ *solves the heat equation (2.2) with the initial and boundary value condition (2.3). Define*

$$\tilde{\psi}(\boldsymbol{x}, t) \triangleq \psi(\boldsymbol{F}^{-1}(\boldsymbol{x}), t),\ \tilde{\kappa}(\boldsymbol{x}) \triangleq |D\boldsymbol{F}(\boldsymbol{F}^{-1}(\boldsymbol{x}))|\kappa(\boldsymbol{F}^{-1}(\boldsymbol{x})),$$

$$\tilde{S}(\boldsymbol{x},t) \triangleq |D\boldsymbol{F}(\boldsymbol{F}^{-1}(\boldsymbol{x}))|^{-1} S(\boldsymbol{F}^{-1}(\boldsymbol{x}),t),\ \tilde{A}(\boldsymbol{x}) = \boldsymbol{F}_* \boldsymbol{A}(\boldsymbol{x}) \triangleq \frac{D\boldsymbol{F}\boldsymbol{A}D\boldsymbol{F}^T}{|D\boldsymbol{F}|} \circ \boldsymbol{F}^{-1}(\boldsymbol{x}),$$

then $\tilde{\psi}(\boldsymbol{x},t)$ *solves (2.2) with* $\tilde{\kappa}(\boldsymbol{x})$, $\tilde{\boldsymbol{A}}(\boldsymbol{x})$ *and* $\tilde{S}(\boldsymbol{x},t)$. *Also the two systems give the same out-coming heat flow at the boundary, i.e.* $\boldsymbol{\nu} \cdot \boldsymbol{A}\nabla\psi(\boldsymbol{x},t) = \boldsymbol{\nu} \cdot \tilde{\boldsymbol{A}}\nabla\tilde{\psi}(\boldsymbol{x},t)$, $\forall \boldsymbol{x} \in \partial\Omega$.

Proof of Lemma 2. Denote $\boldsymbol{y} = \boldsymbol{F}(\boldsymbol{x})$, according to the definition, the only thing needed to be shown here is that

$$|D\boldsymbol{F}(\boldsymbol{x})|^{-1} \nabla_{\boldsymbol{x}} \cdot (\boldsymbol{A}(\boldsymbol{x})\nabla_{\boldsymbol{x}} u(\boldsymbol{x})) = \nabla_{\boldsymbol{y}} \cdot (\tilde{\boldsymbol{A}}(\boldsymbol{y})\nabla_{\boldsymbol{y}} \tilde{u}(\boldsymbol{y})) = \nabla_{\boldsymbol{y}} \cdot (\boldsymbol{F}_* \boldsymbol{A}(\boldsymbol{y})\nabla_{\boldsymbol{y}} u(\boldsymbol{F}^{-1}(\boldsymbol{y}))) \quad (2.14)$$

We will use the metric argument mentioned above. First when $n \geq 3$, we take the metric $g_{\boldsymbol{A}}$ associated with $\boldsymbol{A}(\boldsymbol{x})$ as in (2.13),

$$g_{\boldsymbol{A}}(\boldsymbol{x}) \triangleq |\boldsymbol{A}(\boldsymbol{x})|^{\frac{1}{n-2}} \boldsymbol{A}(\boldsymbol{x})^{-1}. \quad (2.15)$$

As we have already mentioned above, here are some basic facts which can be verified easily.

- $|g_{\boldsymbol{A}}| = |\boldsymbol{A}|^{\frac{2}{n-2}}$
- $\nabla \cdot (\boldsymbol{A}(\boldsymbol{x})\nabla u(\boldsymbol{x})) = |g_{\boldsymbol{A}}|^{\frac{1}{2}} \Delta_{g_{\boldsymbol{A}}} u = |\boldsymbol{A}|^{\frac{1}{n-2}} \Delta_{g_{\boldsymbol{A}}} u$
- The metric associated with $\tilde{\boldsymbol{A}} = \boldsymbol{F}_* \boldsymbol{A}$ is the pullback of $g_{\boldsymbol{A}}$ by $\boldsymbol{F}^{-1}$, i.e. $g_{\boldsymbol{F}_*\boldsymbol{A}} = (\boldsymbol{F}^{-1})^* g_{\boldsymbol{A}}$. And we have the following $|\boldsymbol{F}_* \boldsymbol{A}(\boldsymbol{y})| = |D\boldsymbol{F}(\boldsymbol{x})|^{2-n} |\boldsymbol{A}(\boldsymbol{x})|$, $|g_{\boldsymbol{F}_*\boldsymbol{A}}(\boldsymbol{y})| = |D\boldsymbol{F}(\boldsymbol{x})|^{-2} |g_{\boldsymbol{A}}(\boldsymbol{x})|$

Then it is easy to see that

$$\begin{aligned} \nabla_{\boldsymbol{x}} \cdot (\boldsymbol{A}(\boldsymbol{x})\nabla_{\boldsymbol{x}} u(\boldsymbol{x})) &= |g_{\boldsymbol{A}}|^{\frac{1}{2}} \Delta_{g_{\boldsymbol{A}}} u = \left(\frac{|g_{\boldsymbol{A}}|}{|(\boldsymbol{F}^{-1})^* g_{\boldsymbol{A}}|}\right)^{\frac{1}{2}} |(\boldsymbol{F}^{-1})^* g_{\boldsymbol{A}}|^{\frac{1}{2}} \Delta_{(\boldsymbol{F}^{-1})^* g_{\boldsymbol{A}}} u \circ \boldsymbol{F}^{-1} \\ &= \left(\frac{|g_{\boldsymbol{A}}|}{|g_{\tilde{\boldsymbol{A}}}|}\right)^{\frac{1}{2}} |g_{\tilde{\boldsymbol{A}}}|^{\frac{1}{2}} \Delta_{g_{\tilde{\boldsymbol{A}}}} u \circ \boldsymbol{F}^{-1} = |D\boldsymbol{F}(\boldsymbol{x})| \nabla_{\boldsymbol{y}} \cdot (\tilde{\boldsymbol{A}}(\boldsymbol{y})\nabla_{\boldsymbol{y}} \tilde{u}(\boldsymbol{y})) \end{aligned}$$

To show that $\boldsymbol{\nu} \cdot \boldsymbol{A}\nabla\psi(\boldsymbol{x},t) = \boldsymbol{\nu} \cdot \tilde{\boldsymbol{A}}\nabla\tilde{\psi}(\boldsymbol{x},t)$, we can either calculate directly, or relate it with the interior product of $\nabla_g u$ and the volume form $d_g V$ since we have the relation

$$(\nabla_g \psi \lrcorner d_g V)|_{\partial\Omega} = (\boldsymbol{\nu} \cdot \boldsymbol{A}\nabla\psi(\boldsymbol{x},t))dS, \quad (2.16)$$

where dS is the Euclidean volume form restricted to $\partial\Omega$. Then we get what we want since $\nabla_g\psi \lrcorner d_g V$ is independent of the choice of coordinates plus the fact that $\boldsymbol{F}$ is identity at the boundary.

When $n = 2$, we can not use the arguments above since (2.15) makes no sense, or from another perspective, in the Laplace-Beltrami operator $\Delta_g = |g|^{-\frac{1}{2}}\nabla\cdot(|g|^{\frac{1}{2}}g^{-1}\nabla)$, determinant of the matrix $|g|^{\frac{1}{2}}g^{-1}$ is always one ($det(|g|^{\frac{1}{2}}g^{-1}) = ((|g|^{\frac{1}{2}})^n|g^{-1}| = |g||g|^{-1} = 1$ since $n = 2$), which is not satisfied by a general $\boldsymbol{A}$. We fix this by first normalizing $\boldsymbol{A}$, define

$$\boldsymbol{A}(\boldsymbol{x}) = |\boldsymbol{A}(\boldsymbol{x})|^{\frac{1}{2}}(\frac{1}{|\boldsymbol{A}(\boldsymbol{x})|^{\frac{1}{2}}}\boldsymbol{A}(\boldsymbol{x})) \triangleq |\boldsymbol{A}(\boldsymbol{x})|^{\frac{1}{2}}\boldsymbol{A}_0(\boldsymbol{x}),$$

so $|\boldsymbol{A}_0| = 1$ and

$$\nabla\cdot(\boldsymbol{A}\nabla u) = \nabla\cdot(|\boldsymbol{A}|^{\frac{1}{2}}\boldsymbol{A}_0\nabla u) = |\boldsymbol{A}|^{\frac{1}{2}}\nabla\cdot(\boldsymbol{A}_0\nabla u) + \nabla|\boldsymbol{A}|^{\frac{1}{2}}\cdot(\boldsymbol{A}_0\nabla u).$$

Then just define the metric associated with $\boldsymbol{A}$ to be $g_{\boldsymbol{A}} = \boldsymbol{A}^{-1}$, we get

$$\nabla\cdot(\boldsymbol{A}(\boldsymbol{x})\nabla u(\boldsymbol{x})) = \Delta_{g_{\boldsymbol{A}}}u + < \nabla_{g_{\boldsymbol{A}}}\log|\boldsymbol{A}|^{\frac{1}{2}}, \nabla_{g_{\boldsymbol{A}}}u >_{g_{\boldsymbol{A}}},$$

and similarly,

$$\nabla\cdot(\tilde{\boldsymbol{A}}(\boldsymbol{y})\nabla\tilde{u}(\boldsymbol{y})) = \Delta_{g_{\tilde{\boldsymbol{A}}}}\tilde{u} + < \nabla_{g_{\tilde{\boldsymbol{A}}}}\log|\tilde{\boldsymbol{A}}|^{\frac{1}{2}}, \nabla_{g_{\tilde{\boldsymbol{A}}}}\tilde{u} >_{g_{\tilde{\boldsymbol{A}}}}.$$

Notice that when $n = 2$, $g_{\tilde{\boldsymbol{A}}} \triangleq \tilde{\boldsymbol{A}}^{-1}$ does not coincides with $(\boldsymbol{F}^{-1})^*(g_{\boldsymbol{A}})$, but satisfies that $g_{\tilde{\boldsymbol{A}}}(\boldsymbol{y}) = |D\boldsymbol{F}(\boldsymbol{x})|(\boldsymbol{F}^{-1})^*g_{\boldsymbol{A}}(\boldsymbol{y})$. Plus the fact that $|\boldsymbol{A}(\boldsymbol{x})| = |\tilde{\boldsymbol{A}}(\boldsymbol{y})|$, we have

$$\Delta_{g_{\tilde{\boldsymbol{A}}}}\tilde{u}(\boldsymbol{y}) = |D\boldsymbol{F}(\boldsymbol{x})|^{-1}\Delta_{g_{\boldsymbol{A}}}u(\boldsymbol{x}),$$

$$< \nabla\log|\tilde{\boldsymbol{A}}|^{\frac{1}{2}}, \nabla\tilde{u} >_{g_{\tilde{\boldsymbol{A}}}}|_{\boldsymbol{y}} = |D\boldsymbol{F}|^{-1} < \nabla\log|\boldsymbol{A}|^{\frac{1}{2}}, \nabla u >_{g_{\boldsymbol{A}}}|_{\boldsymbol{x}},$$

which finishes the proof that $\tilde{\psi}$ solves (2.2) with $\tilde{\kappa}$, $\tilde{\boldsymbol{A}}$ and $\tilde{S}$.

To show $\boldsymbol{\nu}\cdot\boldsymbol{A}\nabla\psi(\boldsymbol{x},t) = \boldsymbol{\nu}\cdot\tilde{\boldsymbol{A}}\nabla\tilde{\psi}(\boldsymbol{x},t)$, we can also either calculate directly or use the same argument above with some small modification. Notice that when $n = 2$, relation (2.16) becomes

$$|g_{\boldsymbol{A}}|^{-\frac{1}{2}}(\nabla_{g_{\boldsymbol{A}}}\psi \lrcorner d_{g_{\boldsymbol{A}}}V)|_{\partial\Omega} = (\boldsymbol{\nu}\cdot\boldsymbol{A}\nabla\psi(\boldsymbol{x},t))dS. \tag{2.17}$$

Then notice that

$$g_{\tilde{\boldsymbol{A}}}(\boldsymbol{y}) = |D\boldsymbol{F}(\boldsymbol{x})|(\boldsymbol{F}^{-1})^* g_{\boldsymbol{A}}(\boldsymbol{y}), \quad |g_{\tilde{\boldsymbol{A}}}(\boldsymbol{y})| = |g_{\boldsymbol{A}}(\boldsymbol{x})|,$$

$$d_{(\boldsymbol{F}^{-1})^* g_{\boldsymbol{A}}} V = |D\boldsymbol{F}|^{-1} d_{g_{\tilde{\boldsymbol{A}}}} V, \quad \nabla_{(\boldsymbol{F}^{-1})^* g_{\boldsymbol{A}}} \tilde{\psi} = |D\boldsymbol{F}| \nabla_{g_{\tilde{\boldsymbol{A}}}} \tilde{\psi},$$

we get

$$\nabla_{g_{\boldsymbol{A}}} \psi \lrcorner d_{g_{\boldsymbol{A}}} V|_{\boldsymbol{x}} = (\nabla_{(\boldsymbol{F}^{-1})^* g_{\boldsymbol{A}}} \psi) \lrcorner d_{(\boldsymbol{F}^{-1})^* g_{\boldsymbol{A}}} V|_{\boldsymbol{y}} = \nabla_{g_{\tilde{\boldsymbol{A}}}} \psi \lrcorner d_{g_{\tilde{\boldsymbol{A}}}} V|_{\boldsymbol{y}}.$$

Combining the fact that $\boldsymbol{F}$ is identity at the boundary, we finish the proof. □

2.5 Determination of the conductivity

In this section, we recover $\boldsymbol{\gamma}$ from $\Sigma_{\boldsymbol{\gamma},\kappa,\boldsymbol{A}}$. We start with a property that will be used to solve the heat equation. Consider the operator $\mathcal{A} \triangleq -\kappa\nabla \cdot (\boldsymbol{A}\nabla)$ in the weighted L^2 space $L^2_{\kappa^{-1}}(\Omega)$ with weight function $\kappa^{-1}(x)$, i.e. the space equipped with the weighted inner product $< u, v >_{\kappa^{-1}} = \int_\Omega u\bar{v}\kappa^{-1}\, d\boldsymbol{x}$, we first set the domain of $\mathcal{A}$ to be $C_0^\infty(\Omega)$ and then extend it to $H_0^1(\Omega) \cap H^2(\Omega)$ by Friedrichs extension. It is well known that, given κ, $\boldsymbol{A}$ both positive with lower bounds strictly greater than zero, $\mathcal{A}$ is positive self-adjoint, furthermore the spectrum of $\mathcal{A}$ consists of real positive eigenvalues $\{\lambda_i\}_{i=1}^\infty$ of finite multiplicity which accumulate at $+\infty$ (we may assume that λ_i is non-decreasing), and the corresponding eigenfunctions $\{\phi_i\}_{i=1}^\infty$ form an orthonormal basis of $L^2_{\kappa^{-1}}(\Omega)$.

And now we return to the topic of this section, determining the conductivity through $\Sigma_{\boldsymbol{\gamma},\kappa,\boldsymbol{A}}$. The method used here has a strong physical interpretation. Recall that for the two dimensional Calderón's inverse problem, we have the following result from A. Nachman [43] stating that anisotropic conductivities are determined by the DtN map $\Lambda_{\boldsymbol{\gamma}}$ up to a boundary-fixing diffeomorphism.

Theorem 2 (Nachman). *Let Ω be a bounded domain in $\mathbf{R}^2$ with C^3 boundary, $\boldsymbol{\gamma}_i \in C^3(\bar{\Omega}, \mathcal{S}^2_{++})$ bounded from below, then if $\Lambda_{\boldsymbol{\gamma}_1} = \Lambda_{\boldsymbol{\gamma}_2}$, there exists a boundary-fixing diffeomorphism $\boldsymbol{F}$ which is at least C^3 such that $\boldsymbol{\gamma}_2 = \boldsymbol{F}_* \boldsymbol{\gamma}_1$.*

Another important fact is that knowing the DtN map $\Lambda_{\boldsymbol{\gamma}}$ is actually equivalent to knowing the quadratic form $Q_{\boldsymbol{\gamma}} : H^{\frac{1}{2}}(\partial\Omega) \to \mathbf{R}$, or the energy functional $E_{\boldsymbol{\gamma}} : H^1(\Omega) \to \mathbf{R}$ induced by $\boldsymbol{\gamma}$ defined as follows

$$Q_{\boldsymbol{\gamma}}(f) = E_{\boldsymbol{\gamma}}(u) = \Lambda_{\boldsymbol{\gamma}} f(f) = \int_{\partial\Omega} u(\boldsymbol{\gamma}\nabla u \cdot \boldsymbol{\nu})\, dS = \int_{\Omega} \nabla u \cdot \boldsymbol{\gamma}\nabla u \, d\boldsymbol{x},$$

where u is the solution to (2.5) with boundary value f. The equivalence can be easily proved since we can recover any one from either one of the other two. The physical interpretation of the value $Q_{\boldsymbol{\gamma}}(f) = E_{\boldsymbol{\gamma}}(u)$ is that, it equals to the amount of energy needed to maintain the boundary voltage f, or to keep the voltage u throughout the domain. We know that energy is conservative, so it must transfer into some other form, which in fact is heat. So it is quite nature to expect that in the static case, the energy used to maintain the voltage should be equal to the heat energy coming out through the boundary, i.e.

$$Q_{\boldsymbol{\gamma}}(f) = E_{\boldsymbol{\gamma}}(u) = -\int_{\partial\Omega} \boldsymbol{A}\nabla\psi_0 \cdot \boldsymbol{\nu}\, dS,$$

where $u(\boldsymbol{x})$, $\psi_0(\boldsymbol{x})$ solve the static conductivity and heat equation. This can be verified as follows,

$$\int_{\partial\Omega} \boldsymbol{A}\nabla\psi_0 \cdot \boldsymbol{\nu}\, dS = \int_{\Omega} \nabla \cdot (\boldsymbol{A}\nabla\psi_0)\, d\boldsymbol{x} = -\int_{\Omega} S(\boldsymbol{x})\, d\boldsymbol{x} = -\int_{\Omega} \nabla u \cdot \boldsymbol{\gamma}\nabla u \, d\boldsymbol{x} = -Q_{\boldsymbol{\gamma}}(f).$$

So we can recover the quadratic form $Q_{\boldsymbol{\gamma}}$ from the static outcoming heat flow. Next we try to recover the static outcoming heat flow from $\Sigma_{\boldsymbol{\gamma},\kappa,\boldsymbol{A}}$ by taking static boundary voltage f, but will get into a problem that the static solution $\psi_0(\boldsymbol{x})$ doesn't satisfy the initial condition. We can fix this by the following result.

Lemma 3. *If we take $f(\boldsymbol{x}, t) = f(\boldsymbol{x})$, then $\lim_{t\to+\infty} \int_{\partial\Omega} (\Sigma_{\boldsymbol{\gamma},\kappa,\boldsymbol{A}} f)(\boldsymbol{x}, t)\, dS = -Q_{\boldsymbol{\gamma}}(f)$.*

Proof of Lemma 3. Assume $u(\boldsymbol{x})$ solves (2.1) with the static boundary data $f(\boldsymbol{x}, t) = f(\boldsymbol{x})$, then the source term will also be static (independent of t), $S(\boldsymbol{x}, t) = S(\boldsymbol{x}) = \nabla u(\boldsymbol{x}) \cdot \boldsymbol{\gamma}\nabla u(\boldsymbol{x})$ and $Q_{\boldsymbol{\gamma}}(f) = \int_{\Omega} S(\boldsymbol{x})\, d\boldsymbol{x}$. After that we solve the heat equation (2.2) by decomposing

$\psi(\boldsymbol{x},t)=\psi_0(\boldsymbol{x})+\psi_1(\boldsymbol{x},t)$, where $\psi_0(\boldsymbol{x})$ solves the static heat equation with the static source term,

$$\nabla\cdot(\boldsymbol{A}\nabla\psi_0(\boldsymbol{x}))+S(\boldsymbol{x})=0,\ \boldsymbol{x}\in\Omega,\quad \psi_0(\boldsymbol{x})=0,\quad \forall\boldsymbol{x}\in\partial\Omega, \tag{2.18}$$

and $\psi_1(\boldsymbol{x},t)$ fixes the initial condition,

$$\kappa^{-1}\partial_t\psi_1=\nabla\cdot(\boldsymbol{A}\nabla\psi_1),\ \psi_1(\boldsymbol{x},0)=-\psi_0(\boldsymbol{x}),\ \forall\boldsymbol{x}\in\Omega,\quad \psi_1(\boldsymbol{x},t)=0,\ \forall\boldsymbol{x}\in\partial\Omega. \tag{2.19}$$

From the standard existence theory, we know there is always a unique $\psi_0(\boldsymbol{x})\in H_0^1(\Omega)$ solves (2.18). Also notice that

$$\int_{\partial\Omega}\boldsymbol{A}\nabla\psi_0\cdot\boldsymbol{\nu}\,dS=\int_\Omega\nabla\cdot(\boldsymbol{A}\nabla\psi_0)\,d\boldsymbol{x}=-\int_\Omega S(\boldsymbol{x})\,d\boldsymbol{x}=-Q_{\boldsymbol{\gamma}}(f).$$

And for ψ_1, we solve it by using the eigenfunction expansion as follows. First we do the eigenfunction decomposition for the initial value $-\psi_0$,

$$-\psi_0(\boldsymbol{x})=\sum_{i=1}^{\infty}a_i\phi_i(\boldsymbol{x}),\quad a_i=<-\psi_0,\phi_i>_{\kappa^{-1}}=-\int_\Omega\psi_0\bar{\phi}_i\kappa^{-1}\,d\boldsymbol{x}. \tag{2.20}$$

Substituting (2.20) into (2.19), we get $\psi_1(\boldsymbol{x},t)=\sum_{i=1}^{\infty}a_ie^{-\lambda_it}\phi_i(\boldsymbol{x})$. Since $\lambda_i\geq\lambda_1>0$, we know that ψ_1 converges to 0 exponentially as $t\to+\infty$, so is the out-coming heat flow corresponding to ψ_1. Then we have

$$\lim_{t\to+\infty}\int_{\partial\Omega}(\Sigma_{\boldsymbol{\gamma},\kappa,\boldsymbol{A}}f)(\boldsymbol{x},t)\,dS=\int_{\partial\Omega}\boldsymbol{A}\nabla\psi_0\cdot\boldsymbol{\nu}\,dS=-Q_{\boldsymbol{\gamma}}(f)$$

. □

This way we recover the quadratic form $Q_{\boldsymbol{\gamma}}$, as well as $\Lambda_{\boldsymbol{\gamma}}$, then since we are working with smooth conductivities within a domain with smooth boundary, by Theorem 2, this determines the conductivity up to a boundary-fixing diffeomorphism which is at least C^3 and proves the following result.

Lemma 4. *If $\Sigma_{\boldsymbol{\gamma}_1,\kappa_1,\boldsymbol{A}_1}=\Sigma_{\boldsymbol{\gamma}_2,\kappa_2,\boldsymbol{A}_2}$, then there exits a boundary-fixing diffeomorphism $\boldsymbol{F}$ of Ω which is at least C^3, s.t. $\boldsymbol{\gamma}_2=\boldsymbol{F}_*\boldsymbol{\gamma}_1$.*

2.6 A density argument

In this section, we prove the density argument mentioned in Section 2.3.

Lemma 5. *Assume $\boldsymbol{\gamma}$ is smooth up to the boundary and bounded below as above, then the space spanned by $\nabla u(\boldsymbol{x}) \cdot \boldsymbol{\gamma}(\boldsymbol{x}) \nabla u(\boldsymbol{x})$, where $u(\boldsymbol{x})$ is arbitrary static solution to (2.1), is dense in $L^2(\Omega)$.*

It is easy to see that

$$span\{\nabla u \cdot \boldsymbol{\gamma} \nabla u\} = span\{\nabla u \cdot \boldsymbol{\gamma} \nabla v\}, \text{ where } u, v \text{ are arbitrary static solutions to (2.1).}$$

So $span\{\nabla u \cdot \boldsymbol{\gamma} \nabla u\}$ is dense if and only if $span\{\nabla u \cdot \boldsymbol{\gamma} \nabla v\}$ is dense, and we will prove the second statement in this section.

$L^2(\Omega)$ is a Hilbert space equipped with the standard L^2 inner product, then any linear subspace is dense if and only if its orthogonal complement contains only the 0 element. So it is equivalent to show that $span\{\nabla u \cdot \boldsymbol{\gamma} \nabla v\}^{\perp} = 0$, i.e. $\forall f(\boldsymbol{x}) \in L^2(\Omega)$ satisfies that $\int_\Omega f(\boldsymbol{x}) \nabla u(\boldsymbol{x}) \cdot \boldsymbol{\gamma}(\boldsymbol{x}) \nabla v(\boldsymbol{x})\, d\boldsymbol{x} = 0$ for u and v being arbitrary static solutions to (2.1), then $f = 0$ (strictly speaking we should use $\bar{f}$ in the inner product, but it doesn't matter here since our final goal is to show $f = 0$).

First we claim that since we are now working on the two dimensional case, we may assume the conductivity $\boldsymbol{\gamma}$ is isotropic, i.e. $\boldsymbol{\gamma} = \gamma(\boldsymbol{x}) I$ based on the following Property proved by J. Sylvester [62].

Property 1 (Sylvester)**.** *Let Ω be a bounded domain in $\mathbf{R}^2$ with C^3 boundary and $\boldsymbol{\gamma} \in C^3(\bar{\Omega}, \mathcal{S}^2_{++})$, then there exits a C^3 domain Ω' and a C^3 diffeomorphism $\boldsymbol{F} : \Omega \to \Omega'$ such that*

$$\forall \boldsymbol{x}' \in \Omega' \quad \boldsymbol{F}_* \boldsymbol{\gamma}(\boldsymbol{x}') = |\boldsymbol{\gamma}(\boldsymbol{F}^{-1}(\boldsymbol{x}'))|^{\frac{1}{2}} I,$$

where I is the identity matrix.

Then for any smooth anisotropic conductivity $\boldsymbol{\gamma}$, we can find a change of coordinates $\boldsymbol{F}$ such that the pushforward $\boldsymbol{F}_* \boldsymbol{\gamma}$ is isotropic. It is easy to verify that

$$\int_\Omega f(\nabla u \cdot \boldsymbol{\gamma} \nabla v)\, d\boldsymbol{x} = \int_{\boldsymbol{F}(\Omega)} f \circ \boldsymbol{F}^{-1} (\nabla (u \circ \boldsymbol{F}^{-1}) \cdot \boldsymbol{F}_* \boldsymbol{\gamma} \nabla (v \circ \boldsymbol{F}^{-1}))\, d\boldsymbol{y},$$

so the density of $span\{\nabla u \cdot \boldsymbol{\gamma} \nabla v\}$ in $L^2(\Omega)$ is equivalent to the density of $span\{\nabla(u \circ \boldsymbol{F}^{-1}) \cdot \boldsymbol{F}_* \boldsymbol{\gamma} \nabla(v \circ \boldsymbol{F}^{-1})\}$ in $L^2(\boldsymbol{F}(\Omega))$, where $\boldsymbol{F}_* \boldsymbol{\gamma}$ is an isotropic conductivity. So from now on, we will assume that $\gamma \in C^\infty(\bar{\Omega})$ is isotropic.

To show that any f statisfies $\int_\Omega f \nabla u \cdot \gamma \nabla v \, d\boldsymbol{x} = 0$, where u and v are arbitrary solutions to the conductivity equation (2.5), is identically 0, we use some special solutions to (2.5). Here is a sketch of the proof.

1. First we use Liouville transform (2.7) and the standard CGO solutions to the related Schrödinger equation, to show that $f\chi_\Omega \in H^{4+\epsilon}(\mathbf{R}^2)$ for $0 < \epsilon < 1$, where χ_Ω is the standard characteristic function of Ω so that $f\chi_\Omega$ is a well defined function on $\mathbf{R}^2$. By Sobolev embedding $H^{4+\epsilon}(\mathbf{R}^2) \subset C^3(\mathbf{R}^2)$, we have $f\chi_\Omega \in C^3(\mathbf{R}^2)$, which implies that f, $\partial_{\boldsymbol{\nu}}^i f$ must vanish at $\partial\Omega$ for $i \leq 3$.

2. Since u, v solve the conductivity equation, we have
$$\nabla u \cdot \gamma \nabla v = \frac{1}{2} \nabla \cdot (\gamma \nabla (uv)).$$
Applying the divergence theorem with the fact that both f and $\partial_{\boldsymbol{\nu}} f$ vanish at the boundary, we have
$$0 = \int_\Omega f \nabla u \cdot \gamma \nabla v \, d\boldsymbol{x} = \frac{1}{2} \int_\Omega f \nabla \cdot (\gamma \nabla (uv)) \, d\boldsymbol{x} = \frac{1}{2} \int_\Omega \nabla \cdot (\gamma \nabla f) uv \, d\boldsymbol{x}.$$
Then we use Liouville transform (2.7) again and the solutions Bukhgeim constructed in [9], to show that $\frac{1}{\gamma} \nabla \cdot (\gamma \nabla (f)) = 0$ in Ω by the same arguments used in [9].

3. Finally based on $\frac{1}{\gamma} \nabla \cdot (\gamma \nabla (f)) = 0$, plus the fact that both f and $\partial_{\boldsymbol{\nu}} f$ vanish at the boundary, we conclude that $f = 0$ by the unique continuation results for elliptic equations.

Step 2 and 3 have already been proven, so the only missing part here is the following.

Lemma 6. *Assume γ is smooth up to boundary as above, $\forall f \in L^2(\Omega)$, s.t. $f \perp span\{\nabla u \cdot \gamma \nabla v\}$, where u, v are arbitrary static solutions to (2.1), then $f\chi_\Omega \in H^{4+\epsilon}(\mathbf{R}^2)$ for any $0 < \epsilon < 1$.*

Recall the Liouville transform (2.7) converts (2.1) into a related Schrödinger equation with potential $q = \frac{\Delta\sqrt{\gamma}}{\sqrt{\gamma}}$, and $u(\boldsymbol{x})$ is a static solution to (2.1) if and only if $u_S(\boldsymbol{x}) = \gamma^{\frac{1}{2}}(\boldsymbol{x})u(\boldsymbol{x})$ solves the Schrödinger equation

$$(-\Delta + q)u_S = 0, \quad u_S|_{\partial\Omega} = g, \tag{2.21}$$

with $g = \gamma^{\frac{1}{2}} f$. In [60], the authors showed that if $g \perp span\{u_S v_S\}$, where u_S and v_S are arbitrary solutions to (2.21), then $g\chi_\Omega \in H^s(\mathbf{R}^2)$ for $0 < s < 1$. They proved this by using pairs of CGO solutions whose product was approximately $e^{i\boldsymbol{k}\cdot\boldsymbol{x}}$ to derive estimates for the Fourier transform of $g\chi_\Omega$ when $|\boldsymbol{k}|$ was large. We extend this result and show that when the potential q is smooth, $g\chi_\Omega$ belongs to $H^s(\mathbf{R}^2)$ for $0 < s < 5$, and we can use almost the same arguments to show that $f\chi_\Omega$ in Lemma 6 belongs to $H^s(\mathbf{R}^2)$, for $0 < s < 5$.

First we review and modify the construction of CGO solutions to the Schrödinger equation (2.21), which were first introduced in [63]. For any given $\boldsymbol{\eta} \in \mathbb{C}^2$ s.t. $\boldsymbol{\eta}\cdot\boldsymbol{\eta} = 0$ and $|\boldsymbol{\eta}|$ large enough, we want to construct CGO solution u_S to (2.21) in the form $u_S(\boldsymbol{x}, \boldsymbol{\eta}) = e^{\boldsymbol{\eta}\cdot\boldsymbol{x}}(1 + r(\boldsymbol{x}, \boldsymbol{\eta}))$, where the correction term $r(\boldsymbol{x}, \boldsymbol{\eta})$ is small in certain norm (like the $W^{1,p}_\delta$ norm or the $H^{n/2+k+\epsilon}$ norm which will be discussed later and the norm is only in $\boldsymbol{x}$ variable).

We introduce some notation here before we move on. $\forall\boldsymbol{\eta} \in \mathbb{C}^2$ satisfies $\boldsymbol{\eta}\cdot\boldsymbol{\eta} = 0$ if and only if $\boldsymbol{\eta} = \frac{1}{2}(\pm\boldsymbol{k}^\perp + i\boldsymbol{k})$ for some $\boldsymbol{k} \in \mathbf{R}^2$ (the factor $\frac{1}{2}$ is just for notation simplicity), where $\boldsymbol{k}^\perp$ stands for the vector obtained by rotating $\boldsymbol{k}$ clockwise by $\frac{\pi}{2}$. We do the analysis for $\boldsymbol{\eta} = \frac{1}{2}(\boldsymbol{k}^\perp + i\boldsymbol{k})$ first, and all the results hold for $\tilde{\boldsymbol{\eta}} = \frac{1}{2}(-\boldsymbol{k}^\perp + i\boldsymbol{k})$ by almost the same arguments with minor adjustments. Then there is a one-to-one correspondence between $\boldsymbol{\eta}$ and $\boldsymbol{k}$, from now on we use $u_S(\boldsymbol{x}, \boldsymbol{k})$ and $r(\boldsymbol{x}, \boldsymbol{k})$ to denote CGO solution and its correction term (just switch the second variable from $\boldsymbol{\eta}$ to $\boldsymbol{k}$). We use $\boldsymbol{k} = (k_1, k_2)^T$ to denote the vector and $k = k_1 + ik_2$ to denote the complex number, similarly $\boldsymbol{x}$ denotes the vector $(x_1, x_2)^T$ and $z = x_1 + ix_2$ denotes the complex number. It is easy to see that $\boldsymbol{\eta}\cdot\boldsymbol{x} = \frac{i}{2}\bar{k}z$ and if we use the standard notation $\partial = \frac{1}{2}(\partial_x - i\partial_y)$, $\bar{\partial} = \frac{1}{2}(\partial_x + i\partial_y)$, then $u_S = e^{\boldsymbol{\eta}\cdot\boldsymbol{x}}(1 + r(\boldsymbol{x}, \boldsymbol{k})) = e^{\frac{i}{2}\bar{k}z}(1 + r(\boldsymbol{x}, \boldsymbol{k}))$ solves the Schrödinger equation (2.21) is equivalent to $(\Delta + 2\boldsymbol{\eta}\cdot\nabla - q)r = q$,

or written in complex notation

$$(4\bar{\partial}\partial + 2i\bar{k}\bar{\partial} - q)r = q. \tag{2.22}$$

This was solved in [63] by constructing $r(\boldsymbol{x}, \boldsymbol{k})$ explicitly with the following expansion,

$$r(\boldsymbol{x}, \boldsymbol{k}) = \frac{a(\boldsymbol{x})}{i\bar{k}} + \frac{b(\boldsymbol{x}, \boldsymbol{k})}{(i\bar{k})^2}, \tag{2.23}$$

where we have uniform bounds (in $\boldsymbol{k}$) for the norm of $b(\boldsymbol{x}, \boldsymbol{k})$. And based on this, [60] showed that $\forall g \perp span\{u_S v_S\}$, $g\chi_\Omega \in H^s(\mathbf{R}^2)$ for $0 < s < 1$. To extend their result to any $0 < s < 5$, we need to modify the expansion (2.23) with the following result.

Lemma 7. *Assume q is smooth up to the boundary as above, for $|\boldsymbol{k}|$ large enough and $n \leq 5$, we can construct CGO solutions by solving (2.22) with $r(\boldsymbol{x}, \boldsymbol{k})$ in the following form,*

$$r(\boldsymbol{x}, \boldsymbol{k}) = \sum_{j=1}^{n} \frac{a_j(\boldsymbol{x})}{(i\bar{k})^j} + \frac{b_{n+1}(\boldsymbol{x}, \boldsymbol{k})}{(i\bar{k})^{n+1}}, \tag{2.24}$$

where $a_j = (-2\partial + Pq)^{j-1}Pq$, $j \leq n$ are smooth, do not depend on k and P stands for the Cauchy transform which will be introduced later. Moreover, (2.24) is the unique solution to (2.22) regardless of the value of n.

We call (2.24) CGO solutions expanded up to the $(n-1)$-th order, so (2.23) are CGO solutions expanded up to the 1st order. Equation (2.22) is solved by first formally setting $r = \sum_1^\infty r_j$, where r_j satisfies $(4\bar{\partial}\partial + 2i\bar{k}\bar{\partial})r_j = qr_{j-1}$ with $r_0 = 1$, then proving the summation converges and so solves the equation. Instead of solving (2.22) inside Ω, we extend $q \in C^\infty(\bar{\Omega})$ to $\mathbf{R}^2$ and solve (2.22) on the whole plane. Notice that, there are various way to extend q to the whole plane continuously or even smoothly, which can be done by standard extension techniques, and we require the extension q_{ext} belongs to $C_c^{21}(\mathbf{R}^2)$ at least, the reason will be explained later. We will denote q_{ext} simply by q from now on. Then the key step is to solve the following equation on the whole plane,

$$(4\bar{\partial}\partial + 2i\bar{k}\bar{\partial})r = 2\bar{\partial}(2\partial + i\bar{k})r = f. \tag{2.25}$$

We can first invert the $\bar{\partial}$ equation by the standard Cauchy transform P,

$$Pf(z) = \frac{1}{2\pi} f * \frac{1}{\cdot}(z) = \frac{1}{2\pi} \int_{\mathbf{R}^2} \frac{f(w)}{z-w}\, dw$$

where dw is the usual Lebesgue measure on the plane (we have modified the standard definition by a factor of $\frac{1}{2}$ for simplicity). The properties of P have been studied intensively, like

$$2\bar{\partial}(Pf) = f, \text{ and that } ||Pf||_{W^{1,p}_{\delta}} \leq ||f||_{L^p_{\delta+1}} \tag{2.26}$$

where $1 < p < \infty$, $-\frac{2}{p} < \delta < 1 - \frac{2}{p}$ (see [71] for more details), and $L^p_{\delta+1}$, $W^{1,p}_{\delta}$ are the completion of $C^{\infty}_c(\mathbf{R}^2)$ under the norm

$$||f||_{L^p_{\delta+1}} = (\int_{\mathbf{R}^2} (|f(\boldsymbol{x})|(1+|\boldsymbol{x}|^2)^{\frac{\delta+1}{2}})^p\, d\boldsymbol{x})^{\frac{1}{p}}, \quad ||f||_{W^{1,p}_{\delta}} = ||f||_{L^p_{\delta}} + ||\nabla f||_{L^p_{\delta+1}}.$$

Then we are trying to solve equations like

$$(2\partial + i\bar{k})r = g, \tag{2.27}$$

where $g = Pf$ for (2.25). Notice that $2\partial(e^{i\boldsymbol{k}\cdot\boldsymbol{x}}) = i\bar{k}e^{i\boldsymbol{k}\cdot\boldsymbol{x}}$, using integration factor, we have $(2\partial + i\bar{k})r = e^{-i\boldsymbol{k}\cdot\boldsymbol{x}} 2\partial e^{i\boldsymbol{k}\cdot\boldsymbol{x}} r$, which means $2\partial + i\bar{k}$ is actually 2∂ conjugated by $e^{i\boldsymbol{k}\cdot\boldsymbol{x}}$. Then we can solve (2.27) using $\bar{P}$, which is defined as convolution with $\frac{1}{\bar{z}}$ and has similar properties as P does,

$$r = e^{-i\boldsymbol{k}\cdot\boldsymbol{x}} \bar{P}(e^{i\boldsymbol{k}\cdot\boldsymbol{x}} g). \tag{2.28}$$

But if we solve (2.27) this way, we can not control the norm of r by $|k|$ thus can not prove the convergence of $r = \sum_1^{\infty} r_i$. Instead, [63] solved (2.27) by noticing

$$r = \frac{g}{i\bar{k}} + \frac{r^{(1)}}{i\bar{k}}, \quad \text{where } (2\partial + i\bar{k})r^{(1)} = (-2\partial)g, \tag{2.29}$$

which can be verified by substitute (2.29) into (2.27) directly. Then we have the correct norm control

$$||r||_{W^{1,p}_{\delta}} \leq \frac{C}{|k|} ||g||_{W^{1,p}_{\delta}}, \tag{2.30}$$

from which we can conclude that the summation $r = \sum_1^{\infty} r_i$ converges and we get CGO solutions expanded up to 1st order.

But we can not get CGO solutions expanded up to the n-th order if we solve (2.27) this way. Instead, when g is regular enough, we can modify (2.29) and derive (2.24). If we define $r^{(n)}$ by the following,

$$r = \sum_{j=1}^{n} \frac{(-2\partial)^{j-1} g}{(i\bar{k})^j} + \frac{r^{(n)}}{(i\bar{k})^n}, \tag{2.31}$$

then substitute (2.31) into (2.27), we get

$$(2\partial + i\bar{k})r = g, \quad \Leftrightarrow \quad (2\partial + i\bar{k})r^{(n)} = (-2\partial)^n g. \tag{2.32}$$

And we call (2.31) expanding r up to the n-th order. We remark here that as long as we have enough regularities in g, (2.31) will be the same unique solution (see [63] for the uniqueness proof) to (2.27) in $W^{1,p}_{\delta}$ regardless the value of n. In other words, (2.28), (2.29) and (2.31) are the same solution written in different forms, i.e. $\forall n, m \in \mathbf{N}_+$,

$$r = \frac{g}{i\bar{k}} + \frac{-2\partial g}{(i\bar{k})^2} + ... + \frac{(-2\partial)^{n-1} g}{(i\bar{k})^n} + \frac{r^{(n)}}{(i\bar{k})^n} = \frac{g}{i\bar{k}} + \frac{-2\partial g}{(i\bar{k})^2} + ... + \frac{(-2\partial)^{m-1} g}{(i\bar{k})^m} + \frac{r^{(m)}}{(i\bar{k})^m},$$

as long as $(-2\partial)^n g$ and $(-2\partial)^m g$ exist and belong to $L^p_{\delta+1}$, which is why we require g to be regular enough. And now we are ready to prove Lemma 7.

Proof of Lemma 7. As mentioned above, we first extend $q \in C^{\infty}(\bar{\Omega})$ regularly to the whole plane (at least in $C^{21}_c(\mathbf{R}^2)$), then solve (2.22) in the same way [63] did, i.e. set $r = \sum_1^{\infty} r_j$ with r_j satisfies $(4\bar{\partial}\partial + 2i\bar{k}\bar{\partial})r_j = q r_{j-1}$, where $r_0 = 1$. Since we are constructing the same solutions as [63] and [5] did, all their convergence analysis and norm bounds apply to our solutions as well and we will not repeat the proof but mention some important facts here.

- For $q \in L^{\infty}$ compactly supported, $|k|$ large enough, (2.22) has a unique solution $r \in W^{1,p}_{\delta}(\mathbf{R}^2)$ satisfies the norm estimate $||r||_{W^{1,p}_{\delta}} < \frac{C}{|k|}||q||_{L^{\infty}}$, where the constant C does not depend on k, see [63] for more details.

- Introduce the space H^s_{δ} as the completion of $C^{\infty}_c(\mathbf{R}^2)$ under the norm

$$||f||_{H^s_{\delta}} = (\int_{\mathbf{R}^2} (|(I-\Delta)^{\frac{s}{2}} f)|(1+|\boldsymbol{x}|^2)^{\frac{\delta}{2}})^2 \, d\boldsymbol{x})^{\frac{1}{2}},$$

where $\widehat{(I-\Delta)^{\frac{s}{2}}f})(\boldsymbol{\xi}) = (1+|\boldsymbol{\xi}|^2)^{\frac{s}{2}}\hat{f}(\boldsymbol{\xi})$. Then for $q \in H^{1+l+\epsilon}_{\delta}$ compactly supported, $|k|$ large enough, the unique solution r belongs to $H^{1+l+\epsilon}_{\delta}$, which further implies $r \in C^l(\bar{\Omega})$, and we have norm control $||r||_{H^{1+l+\epsilon}_{\delta}} < \frac{C'}{|k|}||q||_{H^{1+l+\epsilon}_{\delta}}$ where the constant C' does not depend on k, see [5] for more details.

- In both cases, the norm of r_j decays like $||r_j|| \sim \mathcal{O}(\frac{1}{|\boldsymbol{k}|^j})$.

To derive CGO solutions expanded up to the 5-th order, all we need to do is expanding r_j up to higher orders for $j \leq 5$. Namely, we will need to expand r_j up to the $(7-j)$-th order for $j \leq 5$ and leave the rest of r_j unchanged. In fact $\forall n \in \mathbf{N}_+$, we can derive CGO solutions expanded up to the n-th order as long as r_i can be expanded up to order $n+2-i$ for all $i \leq n$, which requires more regularities in q as n increases. As an example, now we show how to derive CGO solutions expanded up to the 2nd order and what we need to do here is just expanding r_1 up to the 3rd order and r_2 up to the 2nd order.

$$\begin{aligned} r_1 =& \frac{Pq}{i\bar{k}} + \frac{-2\partial Pq}{(i\bar{k})^2} + \frac{(-2\partial)^2 Pq}{(i\bar{k})^3} + \frac{r_1^{(3)}}{(i\bar{k})^3} \\ r_2 =& \frac{P(qr_1)}{i\bar{k}} + \frac{-2\partial P(qr_1)}{(i\bar{k})^2} + \frac{r_2^{(2)}}{(i\bar{k})^2} \\ =& \frac{1}{i\bar{k}}P(q\frac{Pq}{i\bar{k}} + q\frac{-2\partial Pq}{(i\bar{k})^2} + q\frac{r_1^{(2)}}{(i\bar{k})^2}) + \frac{1}{(i\bar{k})^2}(-2\partial)P(q\frac{Pq}{i\bar{k}} + q\frac{r_1^{(1)}}{i\bar{k}}) + \frac{r_2^{(2)}}{(i\bar{k})^2}, \end{aligned} \tag{2.33}$$

where $r_1^{(i)}$ solves $(2\partial + i\bar{k})r_1^{(i)} = (-2\partial)^i Pq$, $r_2^{(2)}$ solves $(2\partial + i\bar{k})r_2^{(2)} = (-2\partial)^2 P(qr_1)$. One thing to be noticed here is the facts that P and (-2∂) commute with each other and $q \in C_c^{21}$ actually guarantee that we end up with the same r_i regardless of what order we expand them up to. And by the existing results, the norm of $r_2^{(2)}$ is of order $\mathcal{O}(\frac{1}{|k|^2})$ since the norm of r_1 is of order $\mathcal{O}(\frac{1}{|k|})$. This means the only term that is of order $\mathcal{O}(\frac{1}{|k|^2})$ in the last line of (2.33) is $\frac{Pq(Pq)}{(i\bar{k})^2}$ and we have

$$r_2 = \frac{Pq\,Pq}{(i\bar{k})^2} + \mathcal{O}(\frac{1}{|k|^3}). \tag{2.34}$$

The norm of the rest of r_i, $i \geq 3$ is no more than order $\mathcal{O}(\frac{1}{|k|^3})$, so we have derived CGO

solutions expanded up to the 2nd order, i.e.

$$r(\boldsymbol{x},\boldsymbol{k})=\sum_{1}^{\infty}r_j=\frac{Pq}{i\bar{k}}+\frac{(-2\partial+Pq)Pq}{(i\bar{k})^2}+\frac{b_3(\boldsymbol{x},\boldsymbol{k})}{(i\bar{k})^3}. \tag{2.35}$$

By exactly the same process, but with more terms involved, we can construct CGO solutions expanded up to the n-th order as long as we have enough regularities in q. And for our case, $q\in C_c^{21}$ (the extended version) will be enough since we need C^6 for expanding r_1 up to the 6-th order, then another C^5 for r_2 up to the 5-th order, etc. The expression for a_j can be derived by some easy observation when you write out more terms. □

Remark 3. *With minor adjustments, for each* $\tilde{\boldsymbol{\eta}}=\frac{1}{2}(-\boldsymbol{k}^{\perp}+i\boldsymbol{k})$ *and* $n\leq 5$*, we can construct CGO solutions expanded up to the* n*-th order as follows,*

$$\tilde{r}(\boldsymbol{x},\boldsymbol{k})=\sum_{j=1}^{n}\frac{\tilde{a}_j(\boldsymbol{x})}{(ik)^j}+\frac{\tilde{b}_{n+1}(\boldsymbol{x},\boldsymbol{k})}{(ik)^{n+1}},\quad \tilde{a}_j=(-2\bar{\partial}+\bar{P}q)^{j-1}\bar{P}q, \tag{2.36}$$

as long as we have enough regularities in q*.*

For Lemma 6, we first prove a generalization of the similar result in [60] for the Schrödinger equation. In [60], the authors showed that $\forall g\perp span\{u_Sv_S\}$, $g\chi_\Omega$ was in $H^s(\mathbf{R}^2)$ for $0<s<1$. They used the standard CGO solutions,

$$u_S=e^{(\frac{1}{2}(\boldsymbol{k}^{\perp}+i\boldsymbol{k}))\cdot\boldsymbol{x}}(1+r(\boldsymbol{x},\boldsymbol{k})),\quad v_S=e^{(\frac{1}{2}(-\boldsymbol{k}^{\perp}+i\boldsymbol{k}))\cdot\boldsymbol{x}}(1+\tilde{r}(\boldsymbol{x},\boldsymbol{k})), \tag{2.37}$$

for $|\boldsymbol{k}|$ sufficiently large. Substituting (2.37) back into the assumption $\int_\Omega gu_Sv_S\,d\boldsymbol{x}=0$, they got

$$\int_\Omega ge^{i\boldsymbol{k}\cdot\boldsymbol{x}}(1+r+\tilde{r}+r\tilde{r})\,d\boldsymbol{x}=0\quad\Rightarrow\quad\widehat{g\chi_\Omega}(-\boldsymbol{k})=-\int_\Omega ge^{i\boldsymbol{k}\cdot\boldsymbol{x}}(r+\tilde{r}+r\tilde{r})\,d\boldsymbol{x}. \tag{2.38}$$

Then they used (2.24), (2.36) up to the 1st order to show that $|-\boldsymbol{k}|^s\widehat{g\chi_\Omega}(-\boldsymbol{k})$ was in $L^2(|\boldsymbol{k}|>R)$ for R sufficiently large, which implied $g\chi_\Omega\in H^s(\mathbf{R}^2)$ since only the large $\boldsymbol{k}$ behaviour of $\widehat{g\chi_\Omega}$ mattered. They stopped here since it was enough for their purpose, while we can actually prove $g\chi_\Omega\in H^s$ for some larger s by expanding (2.24), (2.36) up to higher order together with a bootstrapping argument, given that q is regular enough.

For instance, for $|k|$ large enough, if we use CGO solutions (2.24), (2.36) expanded up to the 2nd order, (2.38) becomes

$$
\begin{aligned}
&-\widehat{g\chi_\Omega}(-\boldsymbol{k}) = \frac{1}{i\bar{k}}\widehat{a_1 g\chi_\Omega}(-\boldsymbol{k}) + \frac{1}{ik}\widehat{\tilde{a}_1 g\chi_\Omega}(-\boldsymbol{k}) + \\
&\frac{1}{(i\bar{k})^2}\widehat{a_2 g\chi_\Omega}(-\boldsymbol{k}) + \frac{1}{(ik)^2}\widehat{\tilde{a}_2 g\chi_\Omega}(-\boldsymbol{k}) + \frac{1}{(i\bar{k})(ik)}\widehat{a_1\tilde{a}_1 g\chi_\Omega}(-\boldsymbol{k}) + \\
&\frac{1}{(i\bar{k})(ik)^2}\widehat{a_1\tilde{a}_2 g\chi_\Omega}(-\boldsymbol{k}) + \frac{1}{(i\bar{k})^2(ik)}\widehat{a_2\tilde{a}_1 g\chi_\Omega}(-\boldsymbol{k}) + \frac{1}{(i\bar{k})^2(ik)^2}\widehat{a_2\tilde{a}_2 g\chi_\Omega}(-\boldsymbol{k}) + \\
&\frac{1}{(i\bar{k})^3}\int_\Omega g e^{i\boldsymbol{k}\cdot\boldsymbol{x}} b_3(1+\tilde{r}) + \frac{1}{(ik)^3}\int_\Omega g e^{i\boldsymbol{k}\cdot\boldsymbol{x}}\tilde{b}_3(1+r) - \frac{1}{(i\bar{k})^3(ik)^3}\int_\Omega g e^{i\boldsymbol{k}\cdot\boldsymbol{x}} b_3\tilde{b}_3
\end{aligned}
\tag{2.39}
$$

Then combining with the following facts, we can show that $\forall 0 < s < 2$, $|-\boldsymbol{k}|^s\widehat{g\chi_\Omega}(-\boldsymbol{k}) \in L^2(|\boldsymbol{k}| > R)$, so $g\chi_\Omega \in H^s(\mathbf{R}^2)$.

- The terms in the first line of (2.39), like $\frac{|-\boldsymbol{k}|^s}{i\bar{k}}\widehat{a_1 g\chi_\Omega}(-\boldsymbol{k})$, belongs to $L^2(|\boldsymbol{k}| > R)$ is based on the fact that it has already been shown in [60] that $g\chi_\Omega \in H^t(\mathbf{R}^2)$ for any $0 < t < 1$, plus $g\chi_\Omega$ is compactly supported and $a_1 = Pq$ is regular enough which does not depend on k, then $a_1 g\chi_\Omega \in H^t(\mathbf{R}^2)$, which means $|-\boldsymbol{k}|^t\widehat{a_1 g\chi_\Omega}(-\boldsymbol{k}) \in L^2(|\boldsymbol{k}| > R)$. Then since $|\frac{|-\boldsymbol{k}|^s}{ik}| \leq |\boldsymbol{k}|^{s-1}$ where $s-1 < 1$, so $\frac{|-\boldsymbol{k}|^s}{ik}\widehat{a_1 g\chi_\Omega}(-\boldsymbol{k})$ belongs to $L^2(|\boldsymbol{k}| > R)$.

- The terms in the second and third line of (2.39), like $\frac{|-\boldsymbol{k}|^s}{(i\bar{k})^2}\widehat{a_2 g\chi_\Omega}(-\boldsymbol{k})$, belongs to $L^2(|\boldsymbol{k}| > R)$ since $|\frac{|-\boldsymbol{k}|^s}{(i\bar{k})^2}| < 1$ and the Fourier transform of $a_2 g\chi_\Omega = (-2\partial + Pq)Pq\cdot g\chi_\Omega$ is in $L^2(\mathbf{R}^2)$ (remember a_2 does not depend on k).

- The first two terms in the last line of (2.39), like $\frac{|-\boldsymbol{k}|^s}{(i\bar{k})^3}\int_\Omega g e^{i\boldsymbol{k}\cdot\boldsymbol{x}} b_3(1+\tilde{r})$, belongs to $L^2(|\boldsymbol{k}| > R)$ since $\frac{|-\boldsymbol{k}|^s}{(i\bar{k})^3} \in L^2(|\boldsymbol{k}| > R)$ given that $0 < s < 2$ and the rest $\int_\Omega g(\boldsymbol{x}) b_3(\boldsymbol{x},\boldsymbol{k})(1+\tilde{r}(\boldsymbol{x},\boldsymbol{k}))e^{i\boldsymbol{k}\cdot\boldsymbol{x}}\,d\boldsymbol{x}$ is bounded in $\boldsymbol{k}$ by Cauchy-Schwarz inequality,

  $$|\int_\Omega g(\boldsymbol{x}) b_3(\boldsymbol{x},\boldsymbol{k})(1+\tilde{r}(\boldsymbol{x},\boldsymbol{k}))e^{i\boldsymbol{k}\cdot\boldsymbol{x}}\,d\boldsymbol{x}| \leq ||g||_{L^2(\Omega)}||b_3(\boldsymbol{x},\boldsymbol{k})||_{L^4(\Omega)}||1+\tilde{r}(\boldsymbol{x},\boldsymbol{k})||_{L^4(\Omega)}.$$

  The $L^4(\Omega)$ norm here is in $\boldsymbol{x}$ variable but is uniformly bounded in $\boldsymbol{k}$ and the last higher order term can be bounded similarly which finishes the proof.

To sum up, by using CGO solutions expanded up to the 1st order, the authors proved $g\chi_\Omega \in H^s$ for $0 < s < 1$ in [60]. Based on this and continue to expand CGO solutions up to the 2nd order, we prove $g\chi_\Omega \in H^s$ for $0 < s < 2$. The reason we need to expand CGO solutions to the next order is that we want the second order terms in r and $\tilde{r}$ to be independent of k so we can bound them like we did above. Then as long as q is regular enough to expand CGO solutions to higher order, we can keep running this bootstrapping process to get more and more regularities in $g\chi_\Omega$. Similar with Lemma 6, if we want to show $g\chi_\Omega$ belongs to H^s for $s < 5$, then we will need to use CGO solutions expanded up to the 5-th order which requires q (the extended version) belongs to $C_c^{21}(\mathbf{R}^2)$ at least as stated above. Now we come back to the conductivity equation and prove Lemma 6.

Proof of Lemma 6. As mentioned above, we take solutions to the conductivity equation (2.1) obtained by using the Liouville transform (2.7) and the CGO solutions constructed to the corresponding Schrödinger equation (2.21), i.e.

$$u = \gamma^{-\frac{1}{2}} e^{(\frac{1}{2}(\boldsymbol{k}^\perp + i\boldsymbol{k}))\cdot \boldsymbol{x}}(1 + r(\boldsymbol{x}, \boldsymbol{k})), \quad v = \gamma^{-\frac{1}{2}} e^{(\frac{1}{2}(-\boldsymbol{k}^\perp + i\boldsymbol{k}))\cdot \boldsymbol{x}}(1 + \tilde{r}(\boldsymbol{x}, \boldsymbol{k})), \tag{2.40}$$

Substituting (2.40) into the assumption $\int_\Omega f\nabla u \cdot \gamma \nabla v \, dx = \frac{1}{2}\int_\Omega f\nabla(\gamma\nabla(uv))\, dx = 0$, we get

$$\begin{aligned}
&\widehat{f\chi_\Omega}(-\boldsymbol{k}) = -\int_\Omega f R e^{i\boldsymbol{k}\cdot\boldsymbol{x}}\, d\boldsymbol{x} + \\
&\frac{2i}{|\boldsymbol{k}|^2}\boldsymbol{k}\cdot\int_\Omega f\nabla R e^{i\boldsymbol{k}\cdot\boldsymbol{x}}\, d\boldsymbol{x} - \frac{i}{|\boldsymbol{k}|^2}\boldsymbol{k}\cdot\int_\Omega f(1+R)\nabla\log\gamma e^{i\boldsymbol{k}\cdot\boldsymbol{x}}\, d\boldsymbol{x} \\
&\frac{1}{|\boldsymbol{k}|^2}\Big(\int_\Omega f(1+R)\Delta\log\gamma e^{i\boldsymbol{k}\cdot\boldsymbol{x}}\, d\boldsymbol{x} + \int_\Omega f\nabla R\cdot\nabla\log\gamma e^{i\boldsymbol{k}\cdot\boldsymbol{x}}\, d\boldsymbol{x} + \int_\Omega f\Delta R e^{i\boldsymbol{k}\cdot\boldsymbol{x}}\, d\boldsymbol{x}\Big),
\end{aligned} \tag{2.41}$$

where $R = R(\boldsymbol{x}, \boldsymbol{k}) = r(\boldsymbol{x}, \boldsymbol{k}) + \tilde{r}(\boldsymbol{x}, \boldsymbol{k}) + r(\boldsymbol{x}, \boldsymbol{k})\tilde{r}(\boldsymbol{x}, \boldsymbol{k})$. The leading order term $\int_\Omega f R e^{i\boldsymbol{k}\cdot\boldsymbol{x}}\, d\boldsymbol{x}$ is exactly the same as what we get in (2.38), so we can run the same bootstrapping arguments to prove $f\chi_\Omega \in H^s(\mathbf{R}^2)$ for $s < 5$. And as we just mentioned above, we need the potential $q = \gamma^{-\frac{1}{2}}\Delta\gamma^{\frac{1}{2}}$ belongs to $C^{21}(\bar{\Omega})$, which is always satisfied since we assume γ to be smooth. □

Next we rephrase a result proved by A. Bukhgeim in [9] that we are going to use later.

Property 2 (Bukhgeim)**.** *Let $\Omega \subset \mathbf{R}^2$ be a bounded domain, $q(\boldsymbol{x})$ be C^2 potential function, then for any C^1 function $f \in C^1(\bar{\Omega})$ and any point $\boldsymbol{x}_0 \in \Omega$, we can construct series of pairs of solutions (u_S^n, v_S^n), which are both at least $C^{1+\alpha}$ for any $\alpha \in [0,1)$, to the Schrödinger equation (2.21), such that*

$$\lim_{n\to+\infty} n \int_\Omega f(\boldsymbol{x}) u_S^n(\boldsymbol{x}) v_S^n(\boldsymbol{x})\, d\boldsymbol{x} = f(\boldsymbol{x}_0).$$

Now we are ready to prove Lemma 5.

Proof of Lemma 5. The lemma is equivalent to that $\forall f \in L^2(\Omega)$, s.t. $f \perp span\{\nabla u \cdot \boldsymbol{\gamma} \nabla v\}$, where u, v are arbitrary static solutions to (2.1), then $f = 0$.

As mentioned above, we may assume the conductivity $\boldsymbol{\gamma}$ is isotropic. By Lemma 6, we have $f\chi_\Omega \in H^{4+\epsilon}(\mathbf{R}^2)$, for $0 < \epsilon < 1$. By Sobolev embedding, $f\chi_\Omega$ belongs to $C^3(\mathbf{R}^2)$, which implies f, $\partial_{\boldsymbol{\nu}}^i f$ $(i \le 3)$ all vanish at the boundary. Then combining the fact that u, v solve (2.1) and applying divergence theorem (which is valid since u, $v \in H^1(\Omega)$), we get

$$0 = \int_\Omega f \nabla u \cdot \gamma \nabla v\, d\boldsymbol{x} = \frac{1}{2}\int_\Omega f \nabla \cdot (\gamma \nabla (uv))\, d\boldsymbol{x} = \frac{1}{2}\int_\Omega \nabla \cdot (\gamma \nabla (f)) uv\, d\boldsymbol{x}. \tag{2.42}$$

Use the Liouville transform (2.7), i.e. $u = \gamma^{-\frac{1}{2}} u_S$, where u_S is the solution to the related Schrödinger equation (2.21), we have $\int_\Omega \frac{1}{\gamma}\nabla \cdot (\gamma \nabla (f)) u_S v_S\, d\boldsymbol{x} = 0$. Since $f \in C^3$ and γ is smooth, $\frac{1}{\gamma}\nabla \cdot (\gamma \nabla (f)) \in C^1(\bar{\Omega})$, then by taking u_S, v_S to be the special solutions constructed in Property 2, we get $\frac{1}{\gamma}\nabla \cdot (\gamma \nabla (f)) = 0$.

Finally by the unique continuation results for elliptic equations, $\frac{1}{\gamma}\nabla \cdot (\gamma \nabla (f)) = 0$ together with both f and $\partial_{\boldsymbol{\nu}} f$ vanish at the boundary, we conclude that $f = 0$. □

2.7 Determination of the heat properties

Consider the heat equation (2.2) and define the source-to-heat flow map $\Phi_{\kappa,\boldsymbol{A}}$ that maps the source $S(\boldsymbol{x}, t)$ to the outcoming heat flow $\boldsymbol{\nu} \cdot \boldsymbol{A} \nabla \psi$, K. Krupchyk, M. Lassas and S. Siltanen [33] proved that this map uniquely determined κ and $\boldsymbol{A}$ with the following result.

Property 3 (Krupchyk, Lassas and Siltanen)**.** *Let $\Omega \subset \mathbf{R}^n$ be a bounded domain with smooth boundary, κ_i, $\boldsymbol{A}_i$ are smooth and bounded from below, then if $\Phi_{\kappa_1,\boldsymbol{A}_1} = \Phi_{\kappa_2,\boldsymbol{A}_2}$, we have $\kappa_1 = \kappa_2$, $\boldsymbol{A}_1 = \boldsymbol{A}_2$. Moreover, use $S_{vs} = \{w(\boldsymbol{x})g(t)|w(\boldsymbol{x}) \in L^2(\Omega)\}$ to denote the space of variable-separated sources, then $\Phi_{\kappa_1,\boldsymbol{A}_1} = \Phi_{\kappa_2,\boldsymbol{A}_2}$ on the space S_{vs} is enough to derive the uniqueness.*

With all these preparations, we are now ready to prove Theorem 1.

Proof of Theorem 1. By Lemma 4, we have already proved that there exits a boundary-fixing diffeomorphism of $\bar{\Omega}$, denote by $\boldsymbol{F}$, such that $\boldsymbol{\gamma}_2 = \boldsymbol{F}_*\boldsymbol{\gamma}_1$. By Lemma 1, we know that $u_1(\boldsymbol{F}^{-1}(\boldsymbol{x}), t)$ solves (2.1) with conductivity $\boldsymbol{F}_*\boldsymbol{\gamma}_1$, which is equal to $\boldsymbol{\gamma}_2$ now. By the uniqueness for the elliptic Dirichlet boundary value problems and the fact that $u_1(\boldsymbol{F}^{-1}(\boldsymbol{x}), t)|_{\partial\Omega} = f$ since $\boldsymbol{F}$ fixes the boundary, we have

$$\begin{aligned} u_2(\boldsymbol{x}, t) =& u_1(\boldsymbol{F}^{-1}(\boldsymbol{x}), t) \\ S_2(\boldsymbol{x}, t) =& \nabla u_2(\boldsymbol{x}, t) \cdot \boldsymbol{\gamma}_2(\boldsymbol{x}) \nabla u_2(\boldsymbol{x}, t) = \nabla u_1(\boldsymbol{F}^{-1}(\boldsymbol{x}), t) \cdot \boldsymbol{F}_*\boldsymbol{\gamma}_1(\boldsymbol{x}) \nabla u_1(\boldsymbol{F}^{-1}(\boldsymbol{x}), t) \\ =& \frac{1}{|D\boldsymbol{F}(\boldsymbol{F}^{-1}(\boldsymbol{x}))|} S_1(\boldsymbol{F}^{-1}(\boldsymbol{x}), t). \end{aligned} \tag{2.43}$$

On the other hand, if we consider a new system with properties $\tilde{\boldsymbol{\gamma}}_1$, $\tilde{\kappa}_1$, $\tilde{\boldsymbol{A}}_1$ defined as in Lemma 1 and Lemma 2,

$$\begin{aligned} &\tilde{\boldsymbol{\gamma}}_1(\boldsymbol{x}) \triangleq \boldsymbol{F}_*\boldsymbol{\gamma}_{\mathbf{1}}(\boldsymbol{x}) = \frac{D\boldsymbol{F}\boldsymbol{A}D\boldsymbol{F}^T}{|D\boldsymbol{F}|} \circ \boldsymbol{F}^{-1}(\boldsymbol{x}), \\ &\tilde{\kappa}_1(\boldsymbol{x}) \triangleq |D\boldsymbol{F}(\boldsymbol{F}^{-1}(\boldsymbol{x}))| \kappa_1(\boldsymbol{F}^{-1}(\boldsymbol{x})),\ \tilde{A}_1(\boldsymbol{x}) \triangleq \boldsymbol{F}_*\boldsymbol{A}_{\mathbf{1}}(\boldsymbol{x}) = \frac{D\boldsymbol{F}\boldsymbol{A}D\boldsymbol{F}^T}{|D\boldsymbol{F}|} \circ \boldsymbol{F}^{-1}(\boldsymbol{x}), \end{aligned} \tag{2.44}$$

and compare $(\tilde{\boldsymbol{\gamma}}_1, \tilde{\kappa}_1, \tilde{\boldsymbol{A}}_1)$ with $(\boldsymbol{\gamma}_2, \kappa_2, \boldsymbol{A}_2)$. We have already pointed out that, $\tilde{\boldsymbol{\gamma}}_1 = \boldsymbol{\gamma}_2 \triangleq \boldsymbol{\gamma}$, so for any input boundary data $f(\boldsymbol{x}, t)$, $\tilde{u}_1(\boldsymbol{x}, t) = u_2(\boldsymbol{x}, t) \triangleq u(\boldsymbol{x}, t)$ which implies $\tilde{S}_1(\boldsymbol{x}, t) = S_2(\boldsymbol{x}, t) \triangleq S(\boldsymbol{x}, t)$. And we have $\Sigma_{\tilde{\boldsymbol{\gamma}}_1,\tilde{\kappa}_1,\tilde{\boldsymbol{A}}_1} = \Sigma_{\boldsymbol{\gamma}_1,\kappa_1,\boldsymbol{A}_1} = \Sigma_{\boldsymbol{\gamma}_2,\kappa_2,\boldsymbol{A}_2}$, where the first equality is by Lemma 1 and Lemma 2 while the second one is our assumption, which means that $\forall S(\boldsymbol{x}, t) = \nabla u(\boldsymbol{x}, t) \cdot \boldsymbol{\gamma}(\boldsymbol{x}) \nabla u(\boldsymbol{x}, t)$, the out-coming heat flows are the same for the two systems. Now we take special boundary input data which is separated in $\boldsymbol{x}$ and t, i.e.

$f(\boldsymbol{x},t) = h(\boldsymbol{x})g(t)$, then the resulting source term $S(\boldsymbol{x},t) = (\nabla u(\boldsymbol{x}) \cdot \boldsymbol{\gamma}(\boldsymbol{x}) \nabla u(\boldsymbol{x}))g(t)$, where $u(\boldsymbol{x})$ is the static solution to (2.1) with boundary value equals h. By Lemma 5 and continuous dependence of the solutions to (2.2) on $S(\boldsymbol{x},t)$, we know that the outcoming heat flows are the same for any source term in the form $S(\boldsymbol{x},t) = w(\boldsymbol{x})g(t)$, where $w(\boldsymbol{x}) \in L^2(\Omega)$. Then by Property 3, we have

$$\kappa_2 = \tilde{\kappa}_1, \quad \boldsymbol{A}_2 = \tilde{\boldsymbol{A}}_1. \tag{2.45}$$

Then by the definition of $\tilde{\kappa}_1$, $\tilde{\boldsymbol{A}}_1$, we finish the proof. □

2.8 Summary

In this chapter, we prove the uniqueness result for a new hybrid method proposed in [33] for the two dimensional case. The main difficulty is to show a density argument, which is proved in Section 2.6. Since the two dimensional anisotropic Calderón's inverse problem is well understood, in this paper we allow the electrical conductivity to be anisotropic and so we can only expect to have uniqueness up to a boundary-fixing diffeomorphism. The hybrid method actually doesn't provide any interior information, so we should not expect any improvement in stability or higher-resolution, but on the other hand, we can recover three coefficients all together and the coupled measurement may be more efficient in application. Further work may include requiring less regularity of the properties, numerical reconstruction, improve the model for time-varying boundary voltage, etc.

Chapter 3

BOUNDARY RECONSTRUCTION USING ONLY THE PET DATA

3.1 Motivation and background

PET is a functional medical imaging modality whose importance is increasing rapidly in disease diagnosis and treatment monitoring. Unlike CT or MRI which provide anatomical structures of the body by reconstructing certain 'static' physical properties, PET provides images of physiologic function by reconstructing distribution of some radioactive tracers that tend to concentrate near metabolic active regions (for example near tumors). It works as follows, before the scan, patients are first injected with some radioactive tracers (for example fludeoxyglucose, an analogue of glucose). After waiting for some time (usually a few hours) for the tracers to distribute throughout the bodies, patients are sent into the PET scanner. Whenever the tracer decays, a positron is emitted and soon annihilates with a nearby electron, which produces two high energy gamma photons travelling in opposite direction along a straight line. These photons sometimes are able to get through the bodies and detected by some detectors on the scanner. Since photons travel at the speed of light, if both two photons generated by the same decay event are captured by some detectors, they will arrive at almost the same time. This means if any two detectors both record getting a photon at the same time, we can conclude that there is a decay event happening at that time somewhere along the line connecting these two detectors. Our goal is to reconstruct the tracers' distribution by counting the numbers of decay events along all the lines connecting a pair of detectors. The total number of decay events along any given line $\boldsymbol{l}$ is proportional to the integral of the distribution function $f \geq 0$ along $\boldsymbol{l}$. But not every decay event can be recorded since the two photons it generated may not both be able to make it to the

detectors due to body attenuation. By Beer's Law and some further calculations, we know that each decay event will be recorded with probability $e^{-\int_{\boldsymbol{l}} g\,ds}$ where $g \geq 0$ is the attenuation coefficient for the body and $\boldsymbol{l}$ is the line along which the two photons generated by the event travel. An important fact to notice here is that the probability only depends on the line, but not the exact position along the line where the decay happens. Then the counting of decay events along any given line $\boldsymbol{l}$ is proportional to

$$\int_{\boldsymbol{l}} f\,ds \cdot e^{-\int_{\boldsymbol{l}} g\,ds} = \mathcal{X}f(\boldsymbol{l})e^{-\mathcal{X}g(\boldsymbol{l})}, \tag{3.1}$$

where $\mathcal{X}$ is the X-ray transform that maps any function $f(\boldsymbol{x})$ to a function defined on the space of all lines that for any given line $\boldsymbol{l}$, $\mathcal{X}f(\boldsymbol{l}) = \int_{\boldsymbol{l}} f(\boldsymbol{x})\,ds$. The X-ray transform $\mathcal{X}$, which is closely related to X-ray and CT scan, is invertible, i.e. we can recover f from $\mathcal{X}f$ using some explicit inversion formula. It has been studied intensively with various efficient reconstruction algorithms that produce thousands of medical images everyday around the world. But for the PET scan, in order to recover f form the data (3.1), we need to first get rid of the term $e^{-\mathcal{X}g(\boldsymbol{l})}$. The process is called attenuation correction to the data and one popular way to do that is by performing another CT scan which reconstructs the body's attenuation coefficient g (strictly speaking, there is a difference between the attenuation coefficient in PET scan and the one in CT scan). Next we can simply multiply the data (3.1) by $e^{\mathcal{X}g(\boldsymbol{l})}$ using the g we just reconstruct to get $\mathcal{X}f$. Then we can finally reconstruct f by inverting $\mathcal{X}f$. We remark here that there are also other reconstructing approaches for the PET scan, such as the probability approach by L. Shepp and Y. Vardi [56], the time-of-flight approach [15], [36] which depends on more advanced hardware, etc. See [18], [50], [67] for more information.

We come across the problem in this chapter during our collaboration with the Imaging Research Laboratory at the University of Washington. They are developing a PET device to examine efficiency of therapies for breast cancers. Instead of using the PET/CT combination mentioned above, they are trying to combine the PET device with standard mammography equipment. Mammography is a projection radiography modality with a low energy point

X-ray source. It is used for early breast cancer detection and roughly speaking, the data it collects is the integral of the attenuation function along all the lines passing through the point source. But these information is not enough for the attenuation correction since mammography is not invertible. Then they wonder if we can first recover the boundary of the breast use the PET and mammography data. The answer is yes and we do not even need the mammography data to do that. Moreover, we show that we can actually recover singularity information about the tracers' distribution function f and the attenuation coefficient g from just the PET data. This can be useful since in medical imaging, usually it is the singularities rather than the exact values of the reconstructed properties that provide important information, like jump discontinuities usually correspond to boundaries of different tissues.

Since usually the reconstruction is performed slice by slice, so in this chapter we only consider the two dimensional case. Then the X-ray transform $\mathcal{X}$ is equivalent with the Radon transform $\mathcal{R}$, which will be defined later, and we switch to Radon notation from now on. The rest of this chapter is organized as follows, in Section 3.2, we review some results about the 2D X-ray/Radon transform and also introduce the Fourier Integral Operator (FIO) and wavefront set, which is the main tool to rigorously describe what we mean by singularities. Then in Section 3.3, we use these tools to show some results under the assumption that both f and g are piecewise smooth functions with jump discontinuities across some closed non-self-intersecting smooth curves. In Section 3.4, we prove the same result for piecewise C^2 functions with jump discontinuities. We show some numerical results in Section 3.5 and summarize the results in Section 3.6.

3.2 Preliminary results

In this section, we review some preliminary results that will be used later in this chapter.

3.2.1 2D X-ray/Radon transform

We first define the Radon transform of $f(\boldsymbol{x}) \in L_c^\infty(\mathbf{R}^n)$ as,

$$\mathcal{R}f(\boldsymbol{\theta}, s) \triangleq \int_{\boldsymbol{x}\cdot\boldsymbol{\theta}=s} f(\boldsymbol{x})\, d\sigma, \quad \boldsymbol{\theta} \in \mathbf{S}^{n-1},\ s \in \mathbf{R}, \tag{3.2}$$

where $d\sigma$ is the Lebesgue measure on the hyperplane $\boldsymbol{x}\cdot\boldsymbol{\theta} = s$. So $\mathcal{R}f$ is a function defined on all the hyperplanes, which are parametrized by the unit normal vector $\boldsymbol{\theta}$ and the distance s to the origin, and returns the integral of f on them. As mentioned above, since we only consider the two dimensional case, hyperplanes are just straight lines which means Radon transform and X-ray transform are the same and we will use Radon notation from now on. Also for any unit vector $\boldsymbol{\theta} \in \mathbf{S}^1$, we can find a unique $\theta \in [0, 2\pi)$, s.t. $\boldsymbol{\theta} = (\cos\theta, \sin\theta)$, so the 2D Radon transform can be viewed as a function defined on $[0, 2\pi) \times \mathbf{R}$.

Introduced by J. Radon [53], the X-ray/Radon transform is the foundation of CT scan and we list some important definitions, properties and results here, see [38], [26], [46], [18] for detailed proofs.

Property 4. *For any $f \in L_c^\infty(\mathbf{R}^n)$, its Radon transform is an even function, i.e. $\mathcal{R}f(\boldsymbol{\theta}, s) = \mathcal{R}f(-\boldsymbol{\theta}, -s)$, for the two dimensional case, if we use the $\theta \in [0, 2\pi)$ notation, the even condition becomes $\mathcal{R}f(\theta, s) = \mathcal{R}f(\theta + \pi, -s)$. Moreover, it satisfies the moments condition: for any non-negative integer k, if we calculate the k-th moment of $\mathcal{R}f$ in s, which is a function of $\boldsymbol{\theta}$, it must be a homogeneous polynomial of degree k in $\boldsymbol{\theta}$ since*

$$M_k(\boldsymbol{\theta}) = \int_{-\infty}^{\infty} \mathcal{R}f(\boldsymbol{\theta}, s) s^k\, ds = \int_{\mathbf{R}^n} f(\boldsymbol{x})(\boldsymbol{x}\cdot\boldsymbol{\theta})^k\, d\boldsymbol{x}.$$

For the two dimensional case, this is equivalent with the following:

$$\forall 0 \le k < l,\ k, l \in \mathbf{Z}, \quad \int_{-\infty}^{\infty} \mathcal{R}f(\theta, s) s^k e^{-il\theta}\, ds d\theta = 0$$

Definition 1. *Define the Radon transpose $\mathcal{R}^T$ that maps a function $g(\boldsymbol{\theta}, s)$ defined on the Radon domain $\mathbf{S}^{n-1} \times \mathbf{R}$ to a function of $\mathbf{R}^n$ as follows,*

$$\mathcal{R}^T g(\boldsymbol{x}) = \int_{\mathbf{S}^{n-1}} g(\boldsymbol{\theta}, \boldsymbol{x}\cdot\boldsymbol{\theta})\, dS,$$

where dS is the surface measure on $\mathbf{S}^{n-1}$. For the two dimensional case using the θ notation,

$$\mathcal{R}^T g(\boldsymbol{x}) = \int_0^{2\pi} g(\theta, \boldsymbol{x}\cdot\boldsymbol{\theta})\, d\theta.$$

Property 5. *For any f that has well-defined Radon transform and Fourier transform,*

$$\widehat{\mathcal{R}f}(\boldsymbol{\theta}, \rho) = (2\pi)^{\frac{n-1}{2}} \hat{f}(\rho\boldsymbol{\theta}), \tag{3.3}$$

where the second hat means Fourier transform and the first hat means the Fourier transform only in the s variable. Similarly, for any even function g on the Radon domain that has well-defined Radon transpose,

$$\widehat{\mathcal{R}^T g}(\boldsymbol{\xi}) = 2(2\pi)^{\frac{n-1}{2}} |\boldsymbol{\xi}|^{1-n} \hat{g}(\frac{\boldsymbol{\xi}}{|\boldsymbol{\xi}|}, |\boldsymbol{\xi}|), \tag{3.4}$$

where the hat on the right hand side is Fourier transform in the second variable.

We remark here that the Fourier transform and its inverse have slightly different definitions with different constants/signs and we are using the following version,

$$\hat{f}(\boldsymbol{\xi}) = (2\pi)^{-\frac{n}{2}} \int_{\mathbf{R}^n} f(\boldsymbol{x}) e^{-i\boldsymbol{x}\cdot\boldsymbol{\xi}}\, d\boldsymbol{x}, \quad \check{f}(\boldsymbol{x}) = (2\pi)^{-\frac{n}{2}} \int_{\mathbf{R}^n} \hat{f}(\boldsymbol{\xi}) e^{i\boldsymbol{x}\cdot\boldsymbol{\xi}}\, d\boldsymbol{\xi}.$$

Theorem 3 (Radon, Ludwig)**.** *For the two dimensional Radon transform, if $g = \mathcal{R}f$, then we have*

$$f = \frac{1}{4\pi}\mathcal{R}^T\mathcal{F}g, \quad \text{or} \quad \frac{1}{4\pi}\mathcal{R}^T\mathcal{F}\mathcal{R} = id, \tag{3.5}$$

where the filter operator $\mathcal{F}$ is the Fourier multiplier on the second variable defined by $\widehat{\mathcal{F}g}(\theta, \rho) = |\rho|\hat{g}(\theta, \rho)$, or equivalently $\mathcal{F} = \mathcal{H}\partial_s$ where $\mathcal{H}$ is the Hilbert transform. Similarly, for any even function g on the Radon domain,

$$\text{If } f \triangleq \frac{1}{4\pi}\mathcal{R}^T\mathcal{F}g \text{ is well defined, } \Rightarrow \mathcal{R}f = g. \tag{3.6}$$

3.2.2 FIO and wavefront set

In this part, we introduce the wavefront set of a distribution, which is used to describe singularities of the distribution, and also review basic definitions, properties of FIO and

microlocal analysis which describe how FIO moves singularities around. While these tools are originally developed by L. Hörmander [27], [28] to solve variable-coefficient linear partial differential equations, they have been applied to inverse problems and received great success, see [68], [48] for examples.

We know that for any compactly supported distribution $u \in \mathcal{E}'(\mathbf{R}^n)$,

$$u \in C_c^\infty(\mathbf{R}^n) \quad \Leftrightarrow \quad \forall \boldsymbol{\xi} \in \mathbf{R}^n,\ \forall N \in \mathbf{Z},\ |\hat{u}(\boldsymbol{\xi})| = O(|\boldsymbol{\xi}|^N),$$

i.e. u is smooth if and only if its Fourier transform (which is well-defined since u is compactly supported) is rapidly decaying in any direction. This motivates the definition of wavefront set which describes both positions and directions where the distribution are not smooth.

Definition 2. *For $u \in \mathcal{D}'(\Omega)$ where Ω is an open subset of $\mathbf{R}^n$. We define the wavefront set of u, denoted by $WF(u) \subset \Omega \times \mathbf{R}^n \setminus \mathbf{0}$, by defining its complement. $(\boldsymbol{x}_0, \boldsymbol{\xi}_0)$ does not belongs $WF(u)$, if there exists a smooth cutoff function $\phi(\boldsymbol{x})$ that is not 0 at $\boldsymbol{x}_0$, an open conic neighbourhood U of $\boldsymbol{\xi}_0$ (conic means if $\boldsymbol{\eta} \in U$, then $t\boldsymbol{\eta} \in U$ for any $t > 0$), such that $\forall \boldsymbol{\xi} \in U$, $\widehat{\phi u}(\boldsymbol{\xi})$ decays rapidly, i.e. faster than any power of $|\boldsymbol{\xi}|$.*

The idea behind the above definition is roughly that we want to analysis the local behaviour of u near some point $\boldsymbol{x}_0 \in \Omega$ by first localizing u by multiplying a cutoff function ϕ, then observing the decay of $\widehat{\phi u}$, which is well-defined since $\phi u \in \mathcal{E}'(\Omega)$. By the definition, $WF(u)$ is a closed conic set in $\Omega \times \mathbf{R}^n \setminus \mathbf{0}$ and it can be proved that

$$\Pi_x WF(u) = singsupp(u),$$

where Π_x is the projection to the x variable and $singsupp(u)$ is the singular support of u, i.e. the complement of the largest open set where u is smooth locally.

But sometimes the wavefront set is not enough since the smooth requirement is too strong. Based on similar ideas, we can define the H^s wavefront set of a distribution u, denoted by $WF_s(u)$, as follows.

Definition 3. *For $u \in \mathcal{D}'(\Omega)$, we define the H^s wavefront set of u, denoted by $WF_s(u) \subset \Omega \times \mathbf{R}^n \setminus \mathbf{0}$, by defining its complement. $(\boldsymbol{x}_0, \boldsymbol{\xi}_0)$ does not belongs $WF_s(u)$, or we say u is*

microlocally in H^s near $(\boldsymbol{x}_0, \boldsymbol{\xi}_0)$, if there exists a smooth cutoff function $\phi(\boldsymbol{x})$ that is not 0 *at $\boldsymbol{x}_0$, an open conic neighbourhood U of $\boldsymbol{\xi}_0$, such that*

$$\int_U |\widehat{\phi u}(\boldsymbol{\xi})|^2 (1 + |\boldsymbol{\xi}|^2)^s \, d\boldsymbol{\xi} < \infty.$$

By definition, $WF_s(u)$ is a closed conic set in $\Omega \times \mathbf{R}^n \setminus \mathbf{0}$ and we have $\forall t < s$, $WF_t(u) \subset WF_s(u) \subset WF(u)$. Roughly speaking, $WF_s(u)$ describes positions and directions where u fail to be $H^s_{loc}(\Omega)$ and we have

$$\Pi_x(WF_s(u)) = H^s - singsupp(u),$$

where $H^s - singsupp(u)$ is the complement of the largest open set where u is $H^s_{loc}(\Omega)$. Also by the Sobolev embedding, we know the larger s is, the less singular the singularities are. See [49] for more discussions about H^s wavefront set.

Another important thing is that how the (H^s) wavefront set changes under change of coordinates. Let Ω' be another open domain in $\mathbf{R}^n$ and $\boldsymbol{F} : \Omega \to \Omega'$ is a diffeomorphism, then for any $u \in \mathcal{D}'(\Omega')$, we define the pull-back distribution $\boldsymbol{F}^* u \in \mathcal{D}'(\Omega)$ as follows

$$\forall \varphi(\boldsymbol{x}) \in C_c^\infty(\Omega), \quad \boldsymbol{F}^* u(\varphi) = u(|det(D\boldsymbol{F}^{-1})| \cdot \varphi \circ \boldsymbol{F}^{-1})$$

and we have the following result.

Property 6. *The (H^s) wavefront set of the pull-back distribution $\boldsymbol{F}^* u$ is given by*

$$WF_{(s)}(\boldsymbol{F}^* u) = \{(\boldsymbol{x}, \boldsymbol{\xi}) \in \Omega \times \mathbf{R}^n \setminus \mathbf{0} | (\boldsymbol{F}(x), (D\boldsymbol{F})^T \boldsymbol{\xi}) \in WF_{(s)}(u)\}. \tag{3.7}$$

This actually shows the invariance of the (H^s) wavefront set which suggests that the whole thing can be intrinsically defined on the cotangent bundle of any manifold.

Next we introduce oscillatory integral $I_{a,\varphi} \in \mathcal{D}'(\Omega)$, which is a family of distributions on $\Omega \subset \mathbf{R}^n$ induced by a phase function φ and a symbol function a. We first define the phase function and space of symbols.

Definition 4. *A real-valued function $\varphi(\boldsymbol{x}, \boldsymbol{\theta}) \in C^\infty(\Omega \times \mathbf{R}^N \setminus \mathbf{0})$ is a phase function if it is positive homogeneous of degree 1 in $\boldsymbol{\theta}$ with nonvanishing gradient, i.e. $\forall (\boldsymbol{x}, \boldsymbol{\theta}) \in \Omega \times \mathbf{R}^N \setminus \mathbf{0}$,*

$\forall t > 0$, *we have* $\varphi(\boldsymbol{x}, t\boldsymbol{\theta}) = t\varphi(\boldsymbol{x}, \boldsymbol{\theta})$ *and* $\nabla_{\boldsymbol{x},\boldsymbol{\theta}}\varphi \neq \mathbf{0}$. *Moreover, a phase function is called non-degenerate if* $\forall(\boldsymbol{x}_0, \boldsymbol{\theta}_0)$ *satisfies* $\nabla_{\boldsymbol{\theta}}\varphi(\boldsymbol{x}_0, \boldsymbol{\theta}_0) = 0$, *we have* $\nabla_{\boldsymbol{x},\boldsymbol{\theta}}\frac{\partial\varphi}{\partial\theta_1}$, $\nabla_{\boldsymbol{x},\boldsymbol{\theta}}\frac{\partial\varphi}{\partial\theta_2}$,..., $\nabla_{\boldsymbol{x},\boldsymbol{\theta}}\frac{\partial\varphi}{\partial\theta_N}$ *are linear independent at* $(\boldsymbol{x}_0, \boldsymbol{\theta}_0)$.

Definition 5. *The space of symbols of order* m *and of type* (ρ, δ), *denoted by* $S^m_{\rho,\delta}(\Omega\times\mathbf{R}^N)$, *is the space of all* $a(\boldsymbol{x}, \boldsymbol{\theta}) \in C^\infty(\Omega\times\mathbf{R}^N)$ *such that for any compact* $K \subset \Omega$ *and any multi-index* $\boldsymbol{\alpha}$, $\boldsymbol{\beta}$, *there is a constant* C *depending on* K, $\boldsymbol{\alpha}$, $\boldsymbol{\beta}$ *and* a *such that*

$$|\partial^{\boldsymbol{\alpha}}_{\boldsymbol{x}}\partial^{\boldsymbol{\beta}}_{\boldsymbol{\theta}}a(\boldsymbol{x}, \boldsymbol{\theta})| \leq C(1 + |\boldsymbol{\theta}|)^{m-\rho|\boldsymbol{\beta}|+\delta|\boldsymbol{\alpha}|}. \tag{3.8}$$

In this thesis, we only use symbols of type $(1, 0)$ and will omit the (ρ, δ) subscripts from now on. Then for any phase function φ and symbol a, we define the oscillatory integral $I_{a,\varphi} \in \mathcal{D}'(\Omega)$ formally as

$$I_{a,\varphi}(\boldsymbol{x}) = \int e^{i\varphi(\boldsymbol{x},\boldsymbol{\theta})}a(\boldsymbol{x}, \boldsymbol{\theta})\, d\boldsymbol{\theta}. \tag{3.9}$$

Clearly this integral does not converge in the usual Lebesgue sense unless $a(\boldsymbol{x}, \boldsymbol{\theta})$ decays fast enough for $\boldsymbol{\theta}$ large, for example when the order of a is less than $-N$. And the whole FIO theory makes sense of (3.9) as a distribution for symbols of any order rigorously, i.e. $\forall u(\boldsymbol{x}) \in C^\infty_c(\Omega)$, we define the value of $I_{a,\varphi}(u(\boldsymbol{x}))$ in a reasonable way such that the resulting $I_{a,\varphi}$ is indeed a distribution and agrees with the normal Lebesgue integral when the order of a is small enough. We do not repeat the official definition here, see [27], [28], [22] for more details. The main idea is that we know from (3.8) $\partial_{\theta_i}a$ decays faster in $\boldsymbol{\theta}$ than a which suggests us to consider integration by parts. By the nonvanishing gradient property of the phase function, we can construct a differential operator L with the following properties: (1) $Le^{i\varphi} = e^{i\varphi}$, (2) $\forall a \in S^m(\Omega \times \mathbf{R}^N)$, $L^T a \in S^{m-1}(\Omega \times \mathbf{R}^N)$, then we define

$$I_{a,\varphi}(u) \triangleq \int e^{i\varphi(\boldsymbol{x},\boldsymbol{\theta})}(L^T)^k(a(\boldsymbol{x}, \boldsymbol{\theta})u(\boldsymbol{x}))\, d\boldsymbol{\theta}d\boldsymbol{x}, \tag{3.10}$$

where k is large enough such that $(L^T)^k(a(\boldsymbol{x}, \boldsymbol{\theta})u(\boldsymbol{x}))$ decays fast enough for the integral to converge. It is easy to proved that the value of (3.10) does not depend on the choice of k as long as the integral converges. Strictly speaking, a is not compactly supported in $\boldsymbol{\theta}$ and

we are actually not allowed to do integration by parts just like this. Another equivalent definition is that take a family of smooth cutoff function $\chi_\epsilon(\boldsymbol{\theta})$ in $\boldsymbol{\theta}$ such that each χ_ϵ is compactly supported, or rapidly decays in any direction and $\forall \boldsymbol{\theta}$, $\chi_\epsilon(\boldsymbol{\theta}) \to 1$ as $\epsilon \to 0$. Then we define

$$I_{a,\varphi}(u) \triangleq \lim_{\epsilon \to 0} \int e^{i\varphi(\boldsymbol{x},\boldsymbol{\theta})} a(\boldsymbol{x},\boldsymbol{\theta}) u(\boldsymbol{x}) \chi_\epsilon(\boldsymbol{\theta})\, d\boldsymbol{\theta} d\boldsymbol{x}, \tag{3.11}$$

where the integral inside the limit clearly converges and it can be proved that the limit exists and does not depend on the choice of χ, also the resulting $I_{a,\varphi}$ is a distribution and it agrees with (3.10). Now with $I_{a,\varphi}$ well-defined as a distribution in Ω, we can study its wavefront set and have the following result.

Theorem 4 (Hörmander)**.** *For a given real-valued non-degenerate phase function φ, define its critical set as $C_\varphi = \{(\boldsymbol{x},\boldsymbol{\theta}) | \nabla_{\boldsymbol{\theta}} \varphi = 0\}$, then C_φ is a closed conic set of codimension N. Consider the map $\boldsymbol{j} : C_\varphi \ni (\boldsymbol{x},\boldsymbol{\theta}) \to (\boldsymbol{x}, \nabla_{\boldsymbol{x}} \varphi(\boldsymbol{x},\boldsymbol{\theta})) \in T^*\Omega$, we have $\forall (\boldsymbol{x},\boldsymbol{\theta}) \in C_\varphi$, $d\boldsymbol{j}(\boldsymbol{x},\boldsymbol{\theta})$ is injective. Define Λ_φ to be the image of C_φ under the map $\boldsymbol{j}$, i.e. $\Lambda_\varphi = \boldsymbol{j}(C_\varphi)$, then we have Λ_φ is a conic Lagrangian submanifold of $T^*\Omega$ with respect to the standard symplectic structure on the cotangent bundle and we call Λ_φ the Lagrangian submanifold parametrized by the phase function φ. For any oscillatory integral $I_{a,\varphi}$ with phase function φ, we have*

$$WF(I_{a,\varphi}) \subset \Lambda_\varphi. \tag{3.12}$$

We remark here we still have $WF(I_{a,\varphi}) \subset \boldsymbol{j}(C_\varphi)$ without the non-degenerate assumption. Moreover, (3.12) only gives a containing relation which can actually be improved: let φ be non-degenerate, for any $(\boldsymbol{x}_0,\boldsymbol{\xi}_0) \in \Lambda_\varphi$, i.e. $\exists (\boldsymbol{x}_0,\boldsymbol{\theta}_0) \in C_\varphi$ s.t. $\boldsymbol{j}(\boldsymbol{x}_0,\boldsymbol{\theta}_0) = (\boldsymbol{x}_0,\boldsymbol{\xi}_0)$, it belongs to $WF(u)$ as long as $a(\boldsymbol{x}_0,\boldsymbol{\theta}_0)$ does not decay rapidly in the $\boldsymbol{\theta}_0$ direction. We can even further determine which H^s wavefront set $(\boldsymbol{x}_0,\boldsymbol{\xi}_0)$ belongs to, see [22] for more detailed discussions.

Now we are ready to introduce FIO. Let $X \subset \mathbf{R}^{n_X}$, $Y \subset \mathbf{R}^{n_Y}$ be open domains, take $\Omega = X \times Y$, then by the Schwartz kernel theorem, any oscillatory integral $I_{a,\varphi} \in \mathcal{D}'(X \times Y)$ induces an operator from $C_c^\infty(Y)$ to $\mathcal{D}'(X)$ and we call it a FIO (induced by $I_{a,\varphi}$), formally

denoted by $\mathcal{A}u = \int e^{i\varphi(\boldsymbol{x},\boldsymbol{y},\boldsymbol{\theta})} a(\boldsymbol{x},\boldsymbol{y},\boldsymbol{\theta}) u(\boldsymbol{y})\, d\boldsymbol{\theta} d\boldsymbol{y}$. By the definition, $\forall v(\boldsymbol{x}) \in C_c^\infty(X)$,

$$\mathcal{A}u(v(\boldsymbol{x})) \triangleq I_{a,\varphi}(v(\boldsymbol{x})u(\boldsymbol{y})) = \int e^{i\varphi(\boldsymbol{x},\boldsymbol{y},\boldsymbol{\theta})} a(\boldsymbol{x},\boldsymbol{y},\boldsymbol{\theta}) v(\boldsymbol{x}) u(\boldsymbol{y})\, d\boldsymbol{\theta} d\boldsymbol{x} d\boldsymbol{y}, \tag{3.13}$$

where the last integral is just a formal notation and should be interpreted as the oscillatory integral $I_{a,\varphi}$. Also we can further define $\mathcal{A}u \in \mathcal{D}'(X)$ for any $u \in \mathcal{E}'(Y)$ if $WF(u)$ satisfies certain conditions. Moreover, the following result tells us how $\mathcal{A}$ moves singularities of u to singularities of $\mathcal{A}u$, i.e. how $WF(\mathcal{A}u)$ is related to $WF(u)$ and $WF(I_{a,\varphi})$, or more generally $WF(K_\mathcal{A})$ where $K_\mathcal{A}$ is the Schwartz kernel of $\mathcal{A}$.

Theorem 5 (Hörmander)**.** *Let $K_\mathcal{A} \in \mathcal{D}'(X \times Y)$ be the Schwartz kernel of the operator $\mathcal{A} : C_c^\infty(Y) \to \mathcal{D}'(X)$. Define the following sets*

$$\begin{aligned}
WF'(K_\mathcal{A}) &= \{(\boldsymbol{x},\boldsymbol{\xi};\boldsymbol{y},-\boldsymbol{\eta}) \in T^*(X \times Y) \setminus \mathbf{0} | (\boldsymbol{x},\boldsymbol{\xi};\boldsymbol{y},\boldsymbol{\eta}) \in WF(K_\mathcal{A})\} \\
WF'_X(K_\mathcal{A}) &= \{(\boldsymbol{x},\boldsymbol{\xi}) \in T^*X \setminus \mathbf{0} | \exists \boldsymbol{y} \in Y, s.t. (\boldsymbol{x},\boldsymbol{\xi};\boldsymbol{y},\mathbf{0}) \in WF'(K_\mathcal{A})\} \\
WF'_Y(K_\mathcal{A}) &= \{(\boldsymbol{y},\boldsymbol{\eta}) \in T^*Y \setminus \mathbf{0} | \exists \boldsymbol{x} \in X, s.t. (\boldsymbol{x},\mathbf{0};\boldsymbol{y},\boldsymbol{\eta}) \in WF'(K_\mathcal{A})\}
\end{aligned}$$

Then $\forall u \in \mathcal{E}'(Y)$ s.t. $WF(u) \cap WF'_Y(K_\mathcal{A}) = \emptyset$, $\mathcal{A}u \in \mathcal{D}'(X)$ is well-defined and we have

$$WF(\mathcal{A}u) \subset WF'(K_\mathcal{A})(WF(u)) \cup WF'_X(K_\mathcal{A}), \tag{3.14}$$

where $WF'(K_\mathcal{A})(\cdot)$ is considered as a relation $T^*Y \to T^*X$, i.e. $\forall U \subset T^*Y$, $WF'(K_\mathcal{A})(U) = \{(\boldsymbol{x},\boldsymbol{\xi}) \in T^*X | \exists (\boldsymbol{y},\boldsymbol{\eta}) \in U, s.t. (\boldsymbol{x},\boldsymbol{\xi};\boldsymbol{y},\boldsymbol{\eta}) \in WF'(K_\mathcal{A})\}$.

Once again since this is a general result, (3.14) only gives a containing relation and we can have more precise statement on $WF(\mathcal{A}u)$ if we put more restrictions on $\mathcal{A}$, for example when $\mathcal{A}$ is a FIO with elliptic symbol, see [28], [49], [17] for more information. Also in the context of $\mathcal{A}$ being a FIO induced by $I_{a,\varphi}$ with φ non-degenerate, define Λ'_φ as

$$\Lambda'_\varphi \triangleq \{(\boldsymbol{x},\boldsymbol{\xi};\boldsymbol{y},-\boldsymbol{\eta}) \in T^*(X \times Y) \setminus \mathbf{0} | (\boldsymbol{x},\boldsymbol{\xi};\boldsymbol{y},\boldsymbol{\eta}) \in \Lambda_\varphi\}$$

and it will be called a homogeneous canonical relation from T^*Y to T^*X which, by the above theorem, controls how singularities move.

3.3 Piecewise smooth case

With all the preparations above, we are now ready to show our results. In this section, we make the following assumptions on the tracers' distribution function f and the attenuation coefficient function g.

Assumption 1. *Assume $f(\boldsymbol{x})$ and $g(\boldsymbol{x})$ have the following form,*

$$f(\boldsymbol{x}) = \sum_{i=1}^{n_f} f_i(\boldsymbol{x})\chi_{\Omega_i}(\boldsymbol{x}) \quad g(\boldsymbol{x}) = \sum_{j=1}^{n_g} g_j(\boldsymbol{x})\chi_{\tilde{\Omega}_j}(\boldsymbol{x}),$$

where $f_i(\boldsymbol{x})$, $g_i(\boldsymbol{x})$ are smooth functions, Ω_i, $\tilde{\Omega}_j$ are bounded open plane domains with smooth boundaries and $\chi_{\Omega_i}(\boldsymbol{x})$ are the characteristic function of Ω_i. Or in other words, f and g are compactly supported, bounded, piecewise smooth functions separated by some closed smooth non-self-intersecting curves. We further assume f and g have non-zero jumps across $\partial\Omega_i$ and $\partial\tilde{\Omega}_j$.

This is a reasonable assumption for our problem with Ω_i, $\tilde{\Omega}_j$ representing different body tissues and our goal is trying to reconstruct their boundaries $\partial\Omega_i$, $\partial\tilde{\Omega}_j$ to the maximum extent using only the PET data $\mathcal{R}fe^{-\mathcal{R}g}$.

We first point out that the algorithm we are proposing here may not be able to recover all of $\partial\Omega_i$ and $\partial\tilde{\Omega}_j$, and we will characterize in detail later in this section which part is missing. Also PET scan does not have uniqueness, i.e. we may have $(f_1, g_1) \neq (f_2, g_2)$ satisfy Assumption 1 with $\mathcal{R}f_1e^{-\mathcal{R}g_1} = \mathcal{R}f_2e^{-\mathcal{R}g_2} \triangleq p$. But the boundaries recovered by our algorithm are valid for all (f, g) with PET data p, in other words, we may not be able to recover all the boundaries, but the ones we get are all correct.

By Assumption 1, we know that $singsupp(f) = \cup\partial\Omega_i$, $singsupp(g) = \cup\partial\tilde{\Omega}_j$, i.e. the boundaries that we want to recover are exactly where f and g are singular. So recovering boundaries is now equivalent with recovering singularities of f and g. This suggests us to first describe singularities of f and g using the tools we just introduce, the wavefront set, then study how the singularities are transferred into the data we collect which is possible

since the Radon transform is actually a FIO and by the corresponding theorems we know how it moves singularities. So the main idea for our algorithm is to first extract singularities of the PET data and then try to recover singularities of f and g based on how they are transferred from one to the other.

The wavefront set of piecewise smooth functions are well understood

$$WF(f) = \{(\boldsymbol{x}, \boldsymbol{\theta}) | \boldsymbol{x} \in \partial\Omega_i, \, \boldsymbol{\theta} \text{ is orthogonal to } \partial\Omega_i \text{ at } \boldsymbol{x}\},$$

which can be easily proved by Theorem 6 using a (local) diffeomorphism to straighten $\partial\Omega_i$. Similar result holds for g.

Next we show that the Radon transform is a FIO by making use of the δ function. First we point out that since $\hat{\delta} = 1$, by Fourier inversion formula, we have

$$\mathcal{E}'(\mathbf{R}^n) \ni \delta(\boldsymbol{x}) = (2\pi)^{-n} \int_{\mathbf{R}^n} e^{i\boldsymbol{x}\cdot\boldsymbol{\xi}} \, d\boldsymbol{\xi},$$

which can actually be interpreted as an oscillatory integral with $\varphi = \boldsymbol{x} \cdot \boldsymbol{\xi}$ and $a = 1$. Then we can rewrite (3.2) as

$$\mathcal{R}f(\boldsymbol{\theta}, s) = \int_{\boldsymbol{x}\cdot\boldsymbol{\theta}=s} f(\boldsymbol{x}) \, d\sigma = \int_{\mathbf{R}^n} f(\boldsymbol{x}) \delta(\boldsymbol{x} \cdot \boldsymbol{\theta} - s) \, d\boldsymbol{x} = \frac{1}{2\pi} \int_{\mathbf{R}^n} \int_{\mathbf{R}} e^{i\mu(\boldsymbol{x}\cdot\boldsymbol{\theta}-s)} f(\boldsymbol{x}) \, d\mu d\boldsymbol{x},$$

which is a FIO with $X = \mathbf{S}^{n-1} \times \mathbf{R}$ ($X = [0, 2\pi) \times \mathbf{R}$ for the 2D case), $Y = \mathbf{R}^n$, $N = 1$, induced by an oscillatory integral $I_{a,\varphi}$ with $\varphi = \rho(\boldsymbol{x} \cdot \boldsymbol{\theta} - s)$ non-degenerate and $a = 1$. Moreover, $\mathcal{R}^T$ is induce by $I_{a,\varphi}$ by simply switch the space X and Y. The critical set and canonical relation of $I_{a,\varphi}$ are given by

$$C_\varphi = \{(\theta, s, \boldsymbol{x}; \mu) | \boldsymbol{x} \cdot \boldsymbol{\theta} - s = 0\}, \quad \Lambda'_\varphi = \{(\theta, \boldsymbol{x} \cdot \boldsymbol{\theta}, \mu \boldsymbol{x} \cdot \boldsymbol{\theta}^\perp, -\mu; \boldsymbol{x}, -\mu\boldsymbol{\theta})\}, \tag{3.15}$$

where $\boldsymbol{\theta}^\perp = (-\sin\theta, \cos\theta)$ is the vector obtained by rotate $\boldsymbol{\theta}$ counterclockwisely by $\frac{\pi}{2}$. By applying (3.14) in Theorem 3.12, we know $\forall \boldsymbol{x_0} \in \partial\Omega_i$, its contribution to $WF(f)$, i.e. $(\boldsymbol{x}_0, \boldsymbol{\xi}_0)$ where $\boldsymbol{\xi}_0$ is orthogonal to $\partial\Omega_i$ at $\boldsymbol{x}_0$, might contribute to $WF(\mathcal{R}f)$ only at $(\theta_0, \boldsymbol{x}_0 \cdot \boldsymbol{\theta}_0, |\boldsymbol{\xi}_0| \boldsymbol{x} \cdot \boldsymbol{\theta}_0^\perp, -|\boldsymbol{\xi}_0|)$ where $\theta_0 \in [0, 2\pi)$ is the unique solution to $\boldsymbol{\theta}_0 = (\cos\theta_0, \sin\theta_0) = \frac{\boldsymbol{\xi}_0}{|\boldsymbol{\xi}_0|}$. Further analysis proves that for the Radon transform, which is an elliptic FIO, (3.14) is

not only a containing relation, but an equality, see [23], [52] for detailed proof of the following result.

Theorem 6 (Guillemin)**.** *Let $f \in \mathcal{E}'(\mathbf{R}^2)$, the correspondence between $WF(f)$ and $WF(\mathcal{R}f)$ is given by*

$$(\boldsymbol{x}_0, \boldsymbol{\xi}_0) \in WF(f), \quad \text{if and only if} \quad (\theta_0, \boldsymbol{x}_0 \cdot \boldsymbol{\theta}_0, |\boldsymbol{\xi}_0| \boldsymbol{x}_0 \cdot \boldsymbol{\theta}_0^{\perp}, -|\boldsymbol{\xi}_0|) \in WF(\mathcal{R}f),$$

where $\boldsymbol{\theta}_0 = (\cos\theta_0, \sin\theta_0) = \frac{\boldsymbol{\xi}_0}{|\boldsymbol{\xi}_0|}$ and they determine each other uniquely. Moreover, f is microlocally in H^s near $(\boldsymbol{x}_0, \boldsymbol{\xi}_0)$ if and only if $\mathcal{R}f$ is microlocally in $H^{s+\frac{1}{2}}$ near $(\theta_0, \boldsymbol{x}_0 \cdot \boldsymbol{\theta}_0, |\boldsymbol{\xi}_0| \boldsymbol{x}_0 \cdot \boldsymbol{\theta}_0^{\perp}, -|\boldsymbol{\xi}_0|)$.

Apply the theorem to our problem, under the current assumption, notice that $(\theta_0, \boldsymbol{x}_0 \cdot \boldsymbol{\theta}_0)$, the Radon domain projection of $(\theta_0, \boldsymbol{x}_0 \cdot \boldsymbol{\theta}_0, |\boldsymbol{\xi}_0| \boldsymbol{x}_0 \cdot \boldsymbol{\theta}_0^{\perp}, -|\boldsymbol{\xi}_0|)$, corresponds exactly to the tangent line of $\partial\Omega_i$ at $\boldsymbol{x}_0$, which means singularities at $\boldsymbol{x}_0 \in \partial\Omega_i$ would transfer to singularities ($\frac{1}{2}$ order smoother) at the exact two points in the Radon domain that representing the tangent line at $\boldsymbol{x}_0$ (since each line in the plane corresponding to two points in the Radon domain). So when we trace along $\partial\Omega_i \subset \mathit{singsupp}(f)$, singularities along the curve will transfer to the Radon domain and trace two 'dual' curves, denoted by $\Gamma_{i,\pm}$, which by the above theorem belong to $\mathit{singsupp}(\mathcal{R}f)$ and the $\pm$ correspond to the two choices of the boundary normal vector, i.e. pointing outwards or inwards. Further analysis actually shows that $WF(\mathcal{R}f)$ is actually consisting of $\Gamma_{i,\pm}$ together with their normal vectors. This one-to-two correspondance has been studied by several authors, [31] gave an algorithm to derive $\partial\Omega_i$ from $\Gamma_{i,\pm}$, [54] showed that $\partial\Omega_i$ and $\Gamma_{i,\pm}$ were actually the Legendre transform of each other, etc. Now we summarize the main results and give another straightforward local method to transfer between $\partial\Omega_i$ and $\Gamma_{i,\pm}$.

Lemma 8. *If f satisfies Assumption 1, then $\mathit{singsupp}(f) = \cup\partial\Omega_i$ and $\mathit{singsupp}(\mathcal{R}f) = \cup\Gamma_{i,\pm}$. Moreover, $\partial\Omega_i$ and $\Gamma_{i,\pm}$ determine each other uniquely and one way to do that is as follows.*

- *From $\partial\Omega_i$ to $\Gamma_{i,\pm}$: assume $\partial\Omega_i$ is given by the parametric equation $(x(t), y(t))$, then $\Gamma_{i,\pm}$ is given by*

$$\begin{aligned}\Gamma_{i,+} &: (\arccos \frac{-y^{'}(t)}{\sqrt{(x^{'}(t))^2 + (y^{'}(t))^2}},\ \frac{x^{'}(t)y(t) - x(t)y^{'}(t)}{\sqrt{(x^{'}(t))^2 + (y^{'}(t))^2}}),\\ \Gamma_{i,-} &: (\arccos \frac{-y^{'}(t)}{\sqrt{(x^{'}(t))^2 + (y^{'}(t))^2}} + \pi,\ -\frac{x^{'}(t)y(t) - x(t)y^{'}(t)}{\sqrt{(x^{'}(t))^2 + (y^{'}(t))^2}})\end{aligned} \tag{3.16}$$

  with possible adjustment on the first angle variable to make it belongs $[0, 2\pi)$.

- *From $\Gamma_{i,\pm}$ to $\partial\Omega_i$: assume $\Gamma_{i,\pm}$ is given by $(\theta(t), s(t))$, then $\partial\Omega_i$ is given by*

$$(\cos\theta(t)s(t) - \frac{s^{'}(t)\sin\theta(t)}{\theta^{'}(t)},\ \sin\theta(t)s(t) + \frac{s^{'}(t)\cos\theta(t)}{\theta^{'}(t)}) \tag{3.17}$$

Proof of Lemma 8. The singular support argument has already been proved above and going from $\partial\Omega_i$ to $\Gamma_{i,\pm}$ is pretty straightforward, just need to calculate the θ and s that representing the tangent line at each point $(x(t), y(t))$.

For the other direction, from the above analysis, each point $(\theta(t), s(t)) \in \Gamma_{i,\pm}$ is related to a point $(x(t), y(t)) \in \partial\Omega_i$ by the tangent line correspondence, which implies $(x(t), y(t))$ is on the line represented by $(\theta(t), s(t))$ on the Radon domain, i.e.

$$x(t)\cos(\theta(t)) + y(t)\sin(\theta(t)) = s(t). \tag{3.18}$$

Then if we differentiate (3.18), we get

$$x^{'}(t)\cos(\theta(t)) + y^{'}(t)\sin(\theta(t)) - x(t)\sin(\theta(t))\theta^{'}(t) + y(t)\cos(\theta(t))\theta^{'}(t) = s^{'}(t). \tag{3.19}$$

Notice that $(x^{'}(t), y^{'}(t))$ is in tangent direction and is orthogonal to the normal vector, we get

$$-x(t)\sin(\theta(t)) + y(t)\cos(\theta(t)) = \frac{s^{'}(t)}{\theta^{'}(t)}. \tag{3.20}$$

Combining (3.18) and (3.20), we can solve $(x(t), y(t))$ and get the result. □

We use RC to denote the set consisting of $\Gamma_{i,\pm}$, i.e. the image of closed non-self-intersecting smooth curves under the map (3.16). We know that any curve Γ in RC is

a curve defined on the infinite cylinder $\mathbf{S}^1 \times \mathbf{R}$ (if we identify $(0, s)$ with $(2\pi, s)$) which is not homotopic to a point path and has no vertical tangent lines. Moreover, though Γ is the image of some smooth curve, it may have some singular points. Further analysis can actually prove that those singular points correspond to the tangent lines at some inflection points of the original curve where the curvature equal 0 and the curve goes from concave up to concave down (or the other way around). Also on the two sides of those singular points, the two pieces are tangent with each other.

Now we return to our original problem, trying to recover $\partial\Omega_i$ and $\partial\tilde{\Omega}_j$ from the PET data $\mathcal{R}fe^{-\mathcal{R}g}$. By Lemma 8, we know $singsupp(\mathcal{R}f) = \cup\Gamma_{i,\pm}$, $singsupp(\mathcal{R}g) = \cup\tilde{\Gamma}_{j,\pm}$, which means $\mathcal{R}f$ and $\mathcal{R}g$ are piecewise smooth functions separated by $\Gamma_{i,\pm}$ and $\tilde{\Gamma}_{j,\pm}$. Since composition of smooth functions are still smooth, we have $e^{-\mathcal{R}g}$ is also a piecewise smooth function separated by $\tilde{\Gamma}_{j,\pm}$. Plus product of smooth functions is still smooth, so our PET data $\mathcal{R}fe^{-\mathcal{R}g}$ is a piecewise smooth function separated by part of $\Gamma_{i,\pm}$ and $\tilde{\Gamma}_{j,\pm}$, i.e.

$$singsupp(\mathcal{R}fe^{-\mathcal{R}g}) \subset (\cup\Gamma_{i,\pm}) \cup (\cup\tilde{\Gamma}_{j,\pm}). \tag{3.21}$$

There are two reasons for (3.21) not being an equality.

- $\forall(\theta_0, s_0) \in \tilde{\Gamma}_{j,\pm}$ such that $\mathcal{R}f(\theta_0, s_0) = 0$, the singularity information about $\tilde{\Gamma}_{j,\pm}$ is lost since the PET data is 0 near (θ_0, s_0). From the above analysis, any point on $\tilde{\Gamma}_{j,\pm}$ corresponds to a point on $\tilde{\Omega}_j$. Assume the corresponding point for (θ_0, s_0) is $\boldsymbol{x}_0 \in \partial\tilde{\Omega}_j$, then this information lost happens since the tangent line of $\partial\tilde{\Omega}_j$ at $\boldsymbol{x}_0$, which is parametrized by (θ_0, s_0) on the Radon domain, does not intersect with the convex hull of $supp(f)$.

- When part of $\Gamma_{i,\pm}$ and $\tilde{\Gamma}_{j,\pm}$ overlap each other, which means $\partial\Omega_i$ and $\partial\tilde{\Omega}_j$ partially overlap each other, the singularity information may be cancelled during multiplication.

We will give an example later in this section to illustrate these two situations. Based on (3.21), we have the following algorithm to recover part of $\partial\Omega_i$ and $\partial\tilde{\Omega}_j$.

Algorithm 1 (Chang). *1. Find singsupp($\mathcal{R}fe^{-\mathcal{R}g}$), the singular support of the PET data, and by (3.21) we have*

$$singsupp(\mathcal{R}fe^{-\mathcal{R}g}) \subset (\cup\Gamma_{i,\pm}) \cup (\cup\tilde{\Gamma}_{j,\pm}). \tag{3.22}$$

2. By Lemma 8, we can calculate part of $\partial\Omega_i$, $\partial\tilde{\Omega}_j$ from singsupp($\mathcal{R}fe^{-\mathcal{R}g}$) by using the local inversion formula (3.17).

And all the above analysis have proved the following main result.

Theorem 7 (Chang). *Given f and g satisfy Assumption 1 with PET data $p(\theta, s) = \mathcal{R}fe^{-\mathcal{R}g}$, Algorithm 1 is able to reconstruct a subset of $(\cup\partial\Omega_i) \cup (\cup\partial\tilde{\Omega}_j)$ just from $p(\theta, s)$, where the missing part is caused by either some tangent lines of $\partial\tilde{\Omega}_j$ do not intersect with the convex hull of supp(f), or part of $\partial\Omega_i$ and $\partial\tilde{\Omega}_j$ overlap each other and the singularity information cancel each other out. Moreover, for any other valid pair (f', g') with the same PET data $p(\theta, s)$, the boundaries recovered by Algorithm 1 are also a subset of $(\cup\partial\Omega_i') \cup (\cup\partial\tilde{\Omega}_j')$, in other words, Algorithm 1 gives the boundaries shared by all pairs of (f, g) with PET data $p(\theta, s)$.*

We close this section by giving an example to illustrate the two reasons that cause information lost: out of range or singularity cancellation. But before that, we need the following result that characterizes the range of the 2D Radon transform restricted to functions satisfy Assumption 1 without the non-zero jump condition. D. Ludwig [38] showed when restricted to Schwartz functions, the range of the Radon transform was the space of all Schwartz functions on the Radon domain (Schwartz in s variable for any $\boldsymbol{\theta} \in \mathbf{S}^{n-1}$) that satisfied the moments condition defined in Proposition 4. We can use similar ideas to show the following result.

Theorem 8 (Chang). *Let X be the space of functions satisfy Assumption 1 without the jump condition, i.e. compactly supported, bounded, piecewise smooth functions separated by some closed smooth non-self-intersecting curves, Y be the space of functions on the Radon domain satisfy the following conditions,*

- $\forall g(\theta, s) \in Y$, *g is compactly supported (in s), bounded.*
- *(even)* $\forall g(\theta, s) \in Y$, $g(\theta, s) = g(\theta + \pi, -s)$.
- *(moments condition)* $\forall g(\theta, s) \in Y$,

$$\forall 0 \leq k < l,\ k, l \in \mathbf{Z}, \quad \int_{-\infty}^{\infty} \mathcal{R}f(\theta, s) s^k e^{-il\theta}\, ds d\theta = 0$$

- $\forall g(\theta, s) \in Y$, *g is piecewise smooth and its singular support consists of some curves from RC which can be further divided into pairs within which either one is the image of the other under the map* $r : (\theta, s) \to (\theta + \pi, -s)$. *If several curves intersect at a point* (θ_0, s_0), *then* $WF(g)$ *at* (θ_0, s_0) *only contains directions that are orthogonal to one of these curves at* (θ_0, s_0).
- $\mathcal{R}^T \mathcal{F} g$ *is well-defined and bounded.*

Then Radon transform gives a one-to-one correspondence between X *and* Y.

Proof of Theorem 8. We already know Radon transform $\mathcal{R}$ is injective and by Property 4 and Theorem 6, it is easy to see that $\forall f(\boldsymbol{x}) \in X$, $\mathcal{R}f \in Y$.

Then it is sufficient to show that $\forall g(\theta, s) \in Y$, there exits $f(\boldsymbol{x}) \in X$, such that $\mathcal{R}f = g$. We prove this by construct f explicitly. Let $f \triangleq \frac{1}{4\pi} \mathcal{R}^T \mathcal{F} g$, since the filter operator $\mathcal{F}$ is an elliptic pseudodifferential operator which does not change $WF(g)$, by similar result to Theorem 6 for $\mathcal{R}^T$, or just apply Theorem 5, we know $singsupp(f)$ is consisting of some smooth curves, which means f is piecewise smooth. We remark here the wavefront set condition for Y at intersection point is important since in general at such intersection point (θ_0, s_0), the wavefront set contains all directions which makes the corresponding backprojection singular along the whole line corresponding to (θ_0, s_0). Next by the same arguments from [38], which made use of the moments condition and applied Paley-Wiener theorem, we can prove f is compactly supported. In the end, we show $\mathcal{R}f = g$ by calculating their Fourier transform using Proposition 5. It is easy to see that a function $h(\theta, s)$ on the Radon domain is even if

and only if $\hat{h}(\theta,\rho)$ (Fourier transform in s variable) is even and if $h(\theta,s)$ is even, $\mathcal{F}h$ is also even. Then we have

$$\mathcal{R}f(\theta,s)=g(\theta,s) \quad \Leftrightarrow \quad \hat{g}(\theta,\rho)=\widehat{\mathcal{R}f}(\theta,\rho)=(2\pi)^{\frac{1}{2}}\hat{f}(\rho\boldsymbol{\theta}),\ \forall\rho,\theta\in\mathbf{R},$$

where the Fourier transform in the first two terms are once again in s variable. By the fact that g is even, it is sufficient to prove

$$\hat{g}(\theta,\rho)=(2\pi)^{\frac{1}{2}}\hat{f}(\rho\boldsymbol{\theta}),\forall\rho>0,\ \theta\in\mathbf{R}.$$

For $\rho>0$, by Proposition 5 and the fact $\mathcal{F}g$ is even, we have

$$\hat{f}(\rho\boldsymbol{\theta})=\frac{1}{4\pi}(2(2\pi)^{\frac{1}{2}}\frac{1}{\rho}\widehat{\mathcal{F}g}(\rho,\theta))=(2\pi)^{-\frac{1}{2}}\frac{1}{\rho}(|\rho|\hat{g}(\rho,\theta))=(2\pi)^{-\frac{1}{2}}\hat{g}(\rho,\theta),$$

which finishes the proof. □

Now consider $g(\boldsymbol{x})=\chi_{B_1}(\boldsymbol{x})$ where B_r is the ball centered at 0 with radius r and χ is the standard characteristic function of a domain, then $singsupp(g)=\partial B_1$ and $\mathcal{R}g(\theta,s)=2\sqrt{1-s^2}\chi_{[-1,1]}(s)$ where multiply $\chi_{[-1,1]}(s)$ means set the function equal 0 for $|s|>1$ (also $\sqrt{1-s^2}$ is not defined for $|s|>1$). Consider the function

$$h(\theta,s)=2\sqrt{4-s^2}\chi_{[-2,2]}(s)e^{-2\sqrt{9-s^2}\chi_{[-3,3]}(s)+2\sqrt{1-s^2}\chi_{[-1,1]}(s)},$$

where multiply characteristic function has the same meaning as above. We claim that $h\in Y$ where Y is the function space defined in Theorem 8. Most conditions are easy to check but the last one needs some more careful calculation of the order and symbol of $\mathcal{R}^T\mathcal{F}g$ as a conormal distribution. Then there exists $f(\boldsymbol{x})\in X$, such that $\mathcal{R}f=h$ and $singsupp(f)=\partial B_2\cup\partial B_1$. But the PET data of (f,g) is

$$p(\theta,s)=\mathcal{R}fe^{-\mathcal{R}g}=2\sqrt{4-s^2}\chi_{[-2,2]}(s)e^{-2\sqrt{9-s^2}\chi_{[-3,3]}(s)}.$$

Apply Algorithm 1 to p, we can recover ∂B_2, but the singularities along ∂B_1 are cancelled out during the multiplication.

Also let $f^{'}(\boldsymbol{x}) = \chi_{B_2}(\boldsymbol{x})$, $g^{'}(\boldsymbol{x}) = \chi_{B_3}(\boldsymbol{x})$, then

$$\mathcal{R}f^{'}e^{-\mathcal{R}g^{'}} = 2\sqrt{4-s^2}\chi_{[-2,2]}(s)e^{-2\sqrt{9-s^2}\chi_{[-3,3]}(s)} = p(\theta, s),$$

i.e. (f, g) and $(f^{'}, g^{'})$ have the same PET data. Clearly $singsupp(f^{'}) = \partial B_2$, $singsupp(g^{'}) = \partial B_3$, and ∂B_2 can be recovered by Algorithm 1 while ∂B_3 is missing since all its tangent lines do not intersect B_2.

Remark 4. *As we can see from the above analysis, the jump condition in Assumption 1 is not really needed in this Section and can be replaced by other conditions like C^k continuous across the boundaries. We add it in to make it more close to the realistic problem and it is also necessary for Section 3.4. Also as we can see from the example, the cancellation only happens when the values of $\mathcal{R}f$ and $e^{-\mathcal{R}g}$ are properly chosen. We make the conjecture that for generic (f, g) pairs, cancellations do not happen.*

3.4 Lower regularities

The piecewise smooth assumption in Assumption 1 is too strong and we try to lower the regularity requirement in this section. The main tool we are going to use is the H^s wavefront set introduced in Section 3.2 and the following relation

$$\forall k \in \mathbf{N}, \quad H^{k+1+\epsilon}(\mathbf{R}^2) \subset C^k(\mathbf{R}^2) \subset H^k_{loc}(\mathbf{R}^2),$$

where the first half is the Sobolev embedding and the second half is by the equivalent definition of $H^k(\mathbf{R}^2)$ for positive integer k. And we can improve Theorem 7 as follows.

Theorem 9 (Chang)**.** *Theorem 7 still holds if we make the following changes:*

- *In Assumption 1, instead of piecewise smooth, let f and g be piecewise C^2.*
- *In Algorithm 1, instead of finding singular support of the PET data in the first step, we find all the (θ, s) where the PET data is not locally C^1 and (3.22) becomes*

$$\{(\theta, s) | \mathcal{R}fe^{-\mathcal{R}g} \text{ is not locally } C^1 \text{ at } (\theta, s)\} \subset (\cup\Gamma_{i,\pm}) \cup (\cup\tilde{\Gamma}_{j,\pm}). \tag{3.23}$$

Proof of Theorem 9. All the analysis from Section 3.3 still holds as long as we can prove (3.23) under the new regularity assumption. First, we characterize the jump along $\partial\Omega_i$ and $\partial\tilde{\Omega}_j$ using the H^s wavefront set. $\forall \boldsymbol{x}_0 \in \partial\Omega$, given f is $C^2 \subset H^2_{loc}$ away from $\partial\Omega_i$ and the non-zero jump condition, it is well known that f is microlocally in H^2 near $(\boldsymbol{x}_0, \boldsymbol{\xi}_0)$ as long as $\boldsymbol{\xi}_0$ is not orthogonal to $\partial\Omega_i$ and if $\boldsymbol{\xi}_0$ is in the normal direction, $(\boldsymbol{x}_0, \boldsymbol{\xi}_0) \in WF_s(f)$ for $s \geq \frac{1}{2}$ which can be shown by straightening $\partial\Omega_i$ locally near $\boldsymbol{x}_0$ together with an integration by parts argument. Since f and g are $C^2 \subset H^2_{loc}$ away from $(\cup\Gamma_{i,\pm}) \cup (\cup\tilde{\Gamma}_{j,\pm})$, we have

$$\begin{aligned} WF_{\frac{1}{2}}(f) &= \{(\boldsymbol{x}, \boldsymbol{\xi}) | \boldsymbol{x} \in \partial\Omega_i, \boldsymbol{\xi} \text{ is the normal vector at } \boldsymbol{x}\}, \\ WF_{\frac{1}{2}}(g) &= \{(\boldsymbol{x}, \boldsymbol{\xi}) | \boldsymbol{x} \in \partial\tilde{\Omega}_j, \boldsymbol{\xi} \text{ is the normal vector at } \boldsymbol{x}\}, \end{aligned} \tag{3.24}$$

and by Theorem 6 they will be transferred to $WF_1(\mathcal{R}f)$ and $WF_1(\mathcal{R}g)$ whose base space projection are $\cup\Gamma_{i,\pm}$ and $\cup\tilde{\Gamma}_{j,\pm}$. This implies $\mathcal{R}f$ and $\mathcal{R}g$ can not be locally C^1 at any point along $\cup\Gamma_{i,\pm}$ and $\cup\tilde{\Gamma}_{j,\pm}$, since $C^1 \subset H^1_{loc}$ implies the H^1 wavefront set should be empty at any locally C^1 point. Then since f is piecewise C^2 away from $\cup\Gamma_{i,\pm}$ and $\mathcal{R}$ smooth things up by $\frac{1}{2}$ order, by Theorem 6 we have $\mathcal{R}f \in H^{\frac{5}{2}}_{loc}$ and is locally C^1 away from $\cup\Gamma_{i,\pm}$. Combining the above results, $\mathcal{R}f$ is at least piecewise C^1 strictly separated by $\cup\Gamma_{i,\pm}$ which means $\mathcal{R}f$ is not locally C^1 at any point along $\cup\Gamma_{i,\pm}$. Same result holds for $\mathcal{R}g$ and we can prove the term $e^{-\mathcal{R}g}$ is also piecewise C^1 strictly separated by $\cup\tilde{\Gamma}_{j,\pm}$ since if not, assume $e^{-\mathcal{R}g}$ is locally C^1 at some $\boldsymbol{x}_0 \in \tilde{\Gamma}_{j,\pm}$, we have $\mathcal{R}g = -ln(e^{-\mathcal{R}g})$ is locally C^1, which contradicts with the above analysis. Then the PET data $\mathcal{R}fe^{-\mathcal{R}g}$ is C^1 away from $(\cup\Gamma_{i,\pm}) \cup (\cup\tilde{\Gamma}_{j,\pm})$. For points in $(\cup\Gamma_{i,\pm}) \cup (\cup\tilde{\Gamma}_{j,\pm})$, the data is not locally C^1 unless $\mathcal{R}f = 0$ or some $\Gamma_{i,\pm}$ overlaps with some $\tilde{\Gamma}_{j,\pm}$ and cancel the singularities during the multiplication. □

3.5 Some numerical results

In this section, we show some numerical results based on the analysis above. For simplicity, we assume f and g satisfy Assumption 1 through this section and we use $p(\theta, s) \triangleq \mathcal{R}fe^{-\mathcal{R}g}$ to represent the PET data of (f, g).

We first use an easy example to illustrate Lemma 8 which shows the correspondence

between the singular curves of f and $\mathcal{R}f$. Figure 3.1 shows a very simple function $f =$

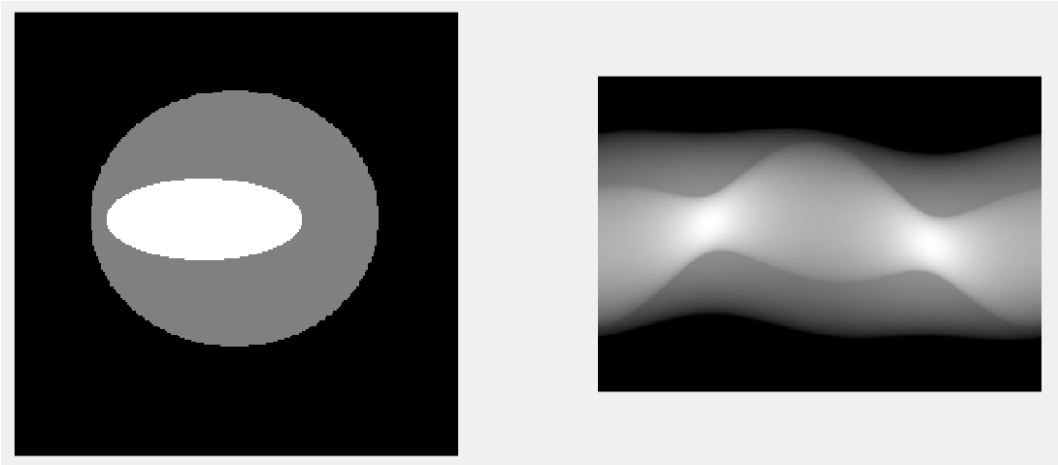

Figure 3.1: Function f (on the left) and its Radon transform (on the right)

$\chi_{ball} + \chi_{ellipsoid}$ (with the origin at the center) and its Radon transform (with $\theta \in [0, 2\pi)$ being the horizontal variable while s being the vertical variable). It is clear that $singsupp(f)$ consists of the circle and the ellipse while we can see four singular curves in its Radon transform, just like Lemma 8 predicts. And the four curves are divided into two groups, the top and bottom curves correspond to the circle while the middle two correspond to the ellipse.

Next we move on to the PET data. Figure 3.1 shows the function $g = \chi_{ball} + \chi_{ellipsoid_2}$, its Radon transform and the PET data $p(\theta, s)$ generated by (f, g). The singular support of g consists of the same circle and a bigger ellipse which together correspond to four singular curves on the Radon domain. When we multiply $\mathcal{R}f$ and $e^{-\mathcal{R}g}$ together, we get 6 singular curves, divided into three groups and corresponding to the circle and two ellipses. Notice that part of the second ellipse is outside the circle, which makes some of its tangent lines not intersect with the convex hull of $supp(f)$ (the ball) and the corresponding information is lost in the PET data.

In order to apply Algorithm 1 numerically, we first need to extract the singular support

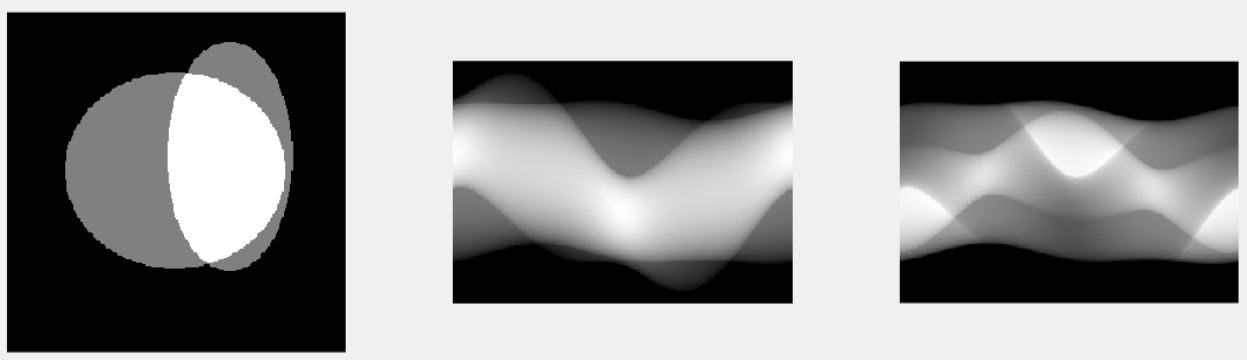

Figure 3.2: Function g (on the left), $\mathcal{R}g$ (in the middle) and the PET data $p(\theta, s)$ (on the right)

of the PET data $p(\theta, s)$. But when given discrete data, how can we find its singular support, what should we look for? Though f and g have jump discontinuities across $(\cup\partial\Omega_i)\cup(\cup\partial\tilde{\Omega}_j)$, their Radon transform may not have similar behaviour across $(\cup\Gamma_{i,\pm})\cup(\cup\tilde{\Gamma}_{j,\pm})$. For example consider $f = \chi_{B_1}$ which has jump discontinuities across ∂B_1, then $\mathcal{R}f(\theta, s) = 2\sqrt{1-s^2}\chi_{[-1,1]}(s)$ and the corresponding singular curve $\Gamma_{1,\pm}$ on the Radon domain is $s = \pm 1$. While $\mathcal{R}f(\theta, s)$ is not differentiable with respect to s at any point along $s = \pm 1$ and $\partial_s\mathcal{R}f(\theta, s)$ blows up near $s = \pm 1$, $\mathcal{R}f$ is actually continuous across $s = \pm 1$. The following corollary, which has already been proved in Theorem 9, tells us what kind of singular behaviour we could expect near the singular support of $p(\theta, s)$.

Corollary 1. *$\forall(\theta_0, s_0) \in singsupp(p(\theta, s))$, $p(\theta, s)$ can not be locally C^1 at (θ_0, s_0), i.e. $p(\theta, s)$ either has a jump discontinuity at (θ_0, s_0), or is not differentiable with respect to θ or s at (θ_0, s_0), which means the limit that defines the derivative might tend to infinite, or does not match from different sides (which ends up to be a jump discontinuity in the partial derivative), or simply does not exist.*

Basically this means at any $(\theta_0, s_0) \in singsupp(p(\theta, s))$, either the function p itself has some notable singular behaviour near (θ_0, s_0), or its first order partial derivative are guaranteed to have some notable singular behaviour near (θ_0, s_0). Then we may try to do some

boundary detections to the discrete p, $\partial_s p$ and $\partial_\theta p$ to extract $singsupp(p(\theta, s))$.

Next we discuss something called non-attenuation-correction (NAC) reconstruction which is an old technique used to reconstruct f before the PET/CT combination came along. The idea is simple, just ignore the attenuation factor in the PET data and apply Radon inversion formula directly to it. Though we can't get f back this way, the images it generated are not

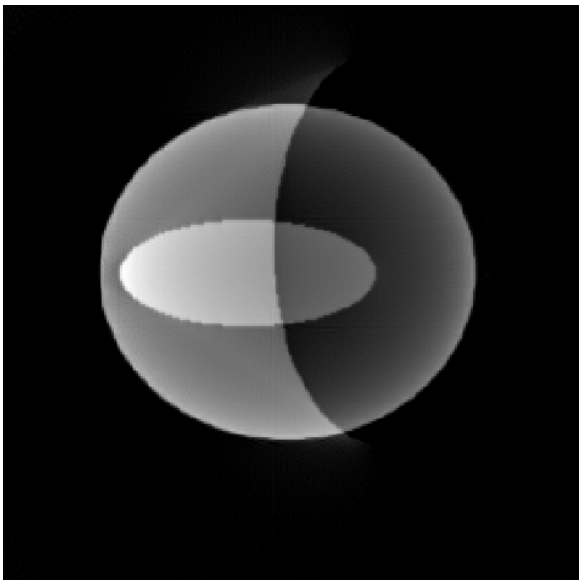

Figure 3.3: A NAC reconstruction of f using the PET data generated by (f, g) defined above

that bad and usually show right structure of the body. The next result states that this is actually not a coincident, the NAC reconstruction can actually give part of the boundaries correctly, maybe plus some artifacts.

Theorem 10 (Chang)**.** *Let $R_{visible}$ be the set of points $\boldsymbol{x}_0 \in \cup\partial\tilde{\Omega}_j$ whose tangent line has non-empty intersection with the convex hull of $supp(f)$. Then singular support of the NAC reconstruction $\frac{1}{4\pi}\mathcal{R}^T\mathcal{F}(p(\theta, s))$ satisfies*

$$singsupp(\frac{1}{4\pi}\mathcal{R}^T\mathcal{F}(p(\theta, s))) \subset (\cup\Omega_i) \cup R_{visible} \cup (\cup L_{ij}), \tag{3.25}$$

where L_{ij} stands for the set of lines that are tangent to both $\partial\Omega_i$ and $\partial\tilde{\Omega}_j$ (might be empty).

Proof of Theorem 10. Let $S_{visible}$ be the set of points $(\theta_0, s_0) \in \cup\tilde{\Gamma}_{j,\pm}$ whose corresponding line $\boldsymbol{x} \cdot \boldsymbol{\theta}_0 = s_0$ has non-empty intersection with the convex hull of $supp(f)$, i.e. $S_{visible} = (\cup\tilde{\Gamma}_{j,\pm}) \cap supp(\mathcal{R}f)$. By previous analysis, we know $p(\theta, s)$ is piecewise smooth separated by $(\cup\Gamma_{i,\pm}) \cup S_{NAC}$. So the wavefront set of p is just $\cup\Gamma_{i,\pm}$, S_{NAC} together with their normal directions except at the intersection point P_{ij} of $\Gamma_{i,\pm}$ and $\tilde{\Gamma}_{j,\pm}$ where the wavefront set usually contains all the directions. Then since the filter operator is an elliptic pseudodifferential operator that does not change the wavefront set and the singular support. $\mathcal{R}^T$ is an elliptic FIO with the same Schwartz kernel, canonical relation as $\mathcal{R}$ but X and Y switched. Results similar to Theorem 6 can be proved for $\mathcal{R}^T$ or simply apply Theorem 5, we have the singularities along $\Gamma_{i,\pm}$ will be transferred to $\partial\Omega_i$, the ones along $S_{visible}$ will be transferred to $R_{visible}$ and the ones at P_{ij} will be transferred to L_{ij}. □

Figure 3.3 shows the NAC reconstruction using the PET data of (f, g) defined above. We can see $singsupp(f)$, i.e. the circle and the small ellipse inside, clearly and also part of $singsupp(g)$, i.e. the circle and part of the big ellipse whose tangent line has non-empty intersection with the circle. Also notice we can see part of the two lines that are tangent to both the circle and the big ellipse just like Theorem 10 predicts.

We also comment on another approach F. Natter and H. Herzog [45] proposed for the attenuation correction. It is based on the moments condition defined in Proposition 4, or sometimes called Helgason-Ludwig consistency condition. The idea is trying to find a function $g^{'}(\boldsymbol{x}) > 0$ such that $p(\theta, s) \cdot e^{\mathcal{R}g^{'}}$ belongs to the range of Radon transform and numerically it is done by making use of the moments condition. In the ideal case, we expect $g^{'} = g$ and $p \cdot e^{\mathcal{R}g^{'}}$ is just $\mathcal{R}f$, then we recover everything. As we have shown above, PET does not have uniqueness, i.e. the above process may end up with some $(f^{'}, g^{'}) \neq (f, g)$, such that

$$p(\theta, s) \cdot e^{\mathcal{R}g^{'}} = \mathcal{R}fe^{-\mathcal{R}g+\mathcal{R}g^{'}} = \mathcal{R}f^{'} \quad \Leftrightarrow \quad \mathcal{R}fe^{-\mathcal{R}g} = \mathcal{R}f^{'}e^{-\mathcal{R}g^{'}},$$

then it seems the whole thing fails. But by Theorem 7, if all we want to recover are $\partial\Omega_i$ and $\partial\tilde{\Omega}_j$, the problem caused by nonuniqueness can be well-controlled. Let A be the boundaries

we recover from $p(\theta, s)$ alone using Algorithm 1, we have proved that A are shared by all (f, g) pairs with PET data $p(\theta, s)$, i.e.

$$A \subset ((\cup\partial\Omega_i) \cup (\cup\partial\tilde{\Omega}_j)), \quad A \subset ((\cup\partial\Omega_i^{'}) \cup (\cup\partial\tilde{\Omega}_j^{'})),$$

so we have

$$A \cap ((\cup\partial\Omega_i^{'}) \cup (\cup\partial\tilde{\Omega}_j^{'})) = A \subset ((\cup\partial\Omega_i) \cup (\cup\partial\tilde{\Omega}_j)),$$

which means if we do a cross validation between the boundaries recovered by $(f^{'}, g^{'})$ and the ones by Algorithm 1, the answers are guaranteed to be correct. We remark here then it seems we can simply calculate A directly and do not need $(f^{'}, g^{'})$ at all. The reason is that Algorithm 1 is still a theoretical algorithm without efficient numerical implementations, while people have made progress on numerically searching for $(f^{'}, g^{'})$, see [45], [44], [72] for more information.

Next we discuss Lamabda tomography, which is a technique for CT reconstruction that focuses on recovering singularities. The idea is given the Radon transform of some function f, consider the following function $g = \Delta\mathcal{R}^T(\mathcal{R}f)$, it can be proved that $\Delta\mathcal{R}^T\mathcal{R}$ is an elliptic pseudodifferential operator of order 1 which not only does not change the wavefront set, but actually enhance singularities. We can actually apply the same idea to our PET data and consider $h = \Delta\mathcal{R}^T(p(\theta, s))$. By the same arguments we used in the proof of Theorem 10, we have the following result.

Corollary 2. *The singular support of the Lambda tomography reconstruction satisfies*

$$singsupp(\Delta\mathcal{R}^T(p(\theta, s))) \subset (\cup\Omega_i) \cup R_{visible} \cup (\cup L_{ij}), \tag{3.26}$$

where $R_{visible}$ and L_{ij} are the same as in Theorem 10.

Figure 3.4 shows the Lambda tomography reconstruction using the same PET data as above. We can see $\cup\Omega_i$ and $R_{visible}$ clearly but the common tangent lines to the circle and big ellipse is not as clear as they are in the NAC reconstruction.

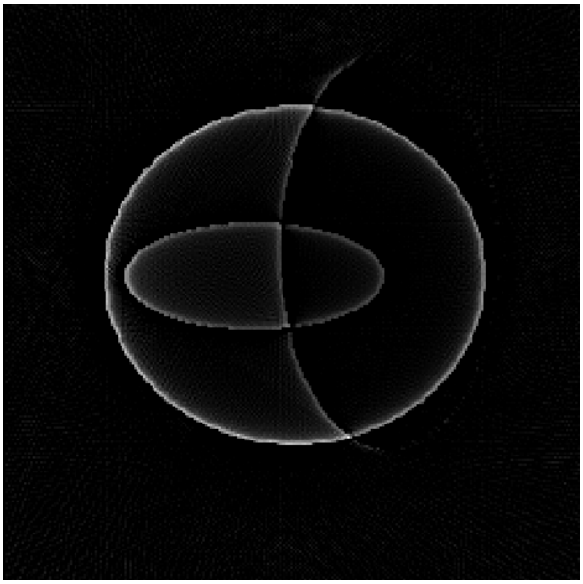

Figure 3.4: A Lambda tomography reconstruction of f using the PET data generated by (f, g) defined above

3.6 Summary

In this chapter, we use FIO and wavefront set theories to show that if $f(\boldsymbol{x})$ and $g(\boldsymbol{x})$ are piecewise C^2 with jump discontinuities across some closed smooth non-self-intersecting curves, then theoretically, we can use just the PET data $p(\theta, s)$ to recover the jump positions for both $f(\boldsymbol{x})$ and $g(\boldsymbol{x})$ unless some of them are out of range or there are some cancellations. But there are still some obstacles to fully implement Algorithm 1 numerically, like the unstable boundary detection and implementing (3.17) efficiently. Also in PET scan, the exact values of $f(\boldsymbol{x})$ actually provide useful information, while our method only recovers singularities. Future work includes stable numerical methods, consider more general domains with less smooth boundaries, etc.

BIBLIOGRAPHY

[1] Giovanni Alessandrini. Stable determination of conductivity by boundary measurements. *Applicable Analysis*, 27(1-3):153–172, 1988.

[2] Kari Astala and Lassi Päivärinta. Calderón's inverse conductivity problem in the plane. *Annals of Mathematics*, pages 265–299, 2006.

[3] Kari Astala, Lassi Päivärinta, and Matti Lassas. Calderón's inverse problem for anisotropic conductivity in the plane. *Communications in Partial Difference Equations*, 30(1-2):207–224, 2005.

[4] Guillaume Bal. Introduction to inverse problems, 2004.

[5] Guillaume Bal and Gunther Uhlmann. Inverse diffusion theory of photoacoustics. *Inverse Problems*, 26(8):085010, 2010.

[6] Guillaume Bal and Gunther Uhlmann. Reconstruction of coefficients in scalar second-order elliptic equations from knowledge of their solutions. *Communications on Pure and Applied Mathematics*, 66(10):1629–1652, 2013.

[7] Russell Brown and Gunther Uhlmann. Uniqueness in the inverse conductivity problem for nonsmooth conductivities in two dimensions. *Communications in partial differential equations*, 22(5-6):1009–1027, 1997.

[8] Russell M Brown and Rodolfo H Torres. Uniqueness in the inverse conductivity problem for conductivities with $\frac{3}{2}$ derivatives in L^p, $p > 2n$. *Journal of Fourier Analysis and Applications*, 9(6):563–574, 2003.

[9] AL Bukhgeim. Recovering a potential from Cauchy data in the two-dimensional case. *Journal of Inverse and Ill-posed Problems*, 16(1):19–33, 2008.

[10] Alberto-P. Calderón. On an inverse boundary value problem. In *Seminar on Numerical Analysis and its Applications to Continuum Physics (Rio de Janeiro, 1980)*, pages 65–73. Soc. Brasil. Mat., Rio de Janeiro, 1980.

[11] B Canuto and O Kavian. Determining coefficients in a class of heat equations via boundary measurements. *SIAM Journal on Mathematical Analysis*, 32(5):963–986, 2001.

[12] Pedro Caro and Keith M. Rogers. Global uniqueness for the Calderón problem with Lipschitz conductivities. *Forum Math. Pi*, 4:e2, 28, 2016.

[13] Jie Chen and Yang Yang. Inverse problem of electro-seismic conversion. *Inverse Problems*, 29(11):115006, 2013.

[14] Margaret Cheney, David Isaacson, and Jonathan C Newell. Electrical impedance tomography. *SIAM review*, 41(1):85–101, 1999.

[15] Michel Defrise, Ahmadreza Rezaei, and Johan Nuyts. Time-of-flight PET data determine the attenuation sinogram up to a constant. *Physics in medicine and biology*, 57(4):885, 2012.

[16] J. J. Duistermaat and L. Hörmander. Fourier integral operators. II. *Acta Math.*, 128(3-4):183–269, 1972.

[17] Johannes Jisse Duistermaat, VW Guillemin, L Hormander, and D Vassiliev. *Fourier integral operators*, volume 2. Springer, 1996.

[18] Charles L Epstein. *Introduction to the mathematics of medical imaging*, volume 102. Siam, 2008.

[19] Adel Faridani, Erik L. Ritman, and Kennan T. Smith. Local tomography. *SIAM J. Appl. Math.*, 52(2):459–484, 1992.

[20] Joel Feldman, Mikko Salo, and Gunther Uhlmann. *The Calderón Problem-An Introduction to Inverse Problems*, volume 1. to appear.

[21] David Dos Santos Ferreira, Carlos E Kenig, Mikko Salo, and Gunther Uhlmann. Limiting Carleman weights and anisotropic inverse problems. *Inventiones mathematicae*, 178(1):119–171, 2009.

[22] Alain Grigis and Johannes Sjöstrand. *Microlocal analysis for differential operators: an introduction*, volume 196. Cambridge University Press, 1994.

[23] Victor Guillemin and Shlomo Sternberg. Some problems in integral geometry and some related problems in micro-local analysis. *American Journal of Mathematics*, 101(4):915–955, 1979.

[24] Boaz Haberman. Uniqueness in Calderóns problem for conductivities with unbounded gradient. *Communications in Mathematical Physics*, 340(2):639–659, 2015.

[25] Boaz Haberman and Daniel Tataru. Uniqueness in Calderóns problem with Lipschitz conductivities. *Duke Mathematical Journal*, 162(3):497–516, 2013.

[26] Sigurdur Helgason. The Radon transform on R^n. In *Integral Geometry and Radon Transforms*, pages 1–62. Springer, 2011.

[27] Lars Hörmander. Fourier integral operators. I. *Acta Math.*, 127(1-2):79–183, 1971.

[28] Lars Hörmander. *The analysis of linear partial differential operators. I–IV*. Springer, Berlin, 1985.

[29] Oleg Yu Imanuvilov and Masahiro Yamamoto. Lipschitz stability in inverse parabolic problems by the Carleman estimate. *Inverse problems*, 14(5):1229, 1998.

[30] Victor Isakov. Some inverse problems for the diffusion equation. *Inverse Problems*, 15(1):3, 1999.

[31] AI Katsevich. Algorithm for recovering discontinuities of a function from its Radon transform. *Applied mathematics letters*, 5(4):73–75, 1992.

[32] Robert Kohn and Michael Vogelius. Determining conductivity by boundary measurements. *Communications on Pure and Applied Mathematics*, 37(3):289–298, 1984.

[33] Katsiaryna Krupchyk, Matti Lassas, and Samuli Siltanen. Determining electrical and heat transfer parameters using coupled boundary measurements. *SIAM Journal on Mathematical Analysis*, 43(5):2096–2115, 2011.

[34] Peter Kuchment and Leonid Kunyansky. Mathematics of thermoacoustic tomography. *European Journal of Applied Mathematics*, 19(02):191–224, 2008.

[35] John M Lee and Gunther Uhlmann. Determining anisotropic real-analytic conductivities by boundary measurements. *Communications on Pure and Applied Mathematics*, 42(8):1097–1112, 1989.

[36] Tom K Lewellen. Time-of-flight PET. In *Seminars in nuclear medicine*, volume 28, pages 268–275. Elsevier, 1998.

[37] Bill Lionheart. Conformal uniqueness results in anisotropic electrical impedance imaging. *Inverse Problems*, 13(1):125, 1997.

[38] Donald Ludwig. The Radon transform on Euclidean space. *Communications on Pure and Applied Mathematics*, 19(1):49–81, 1966.

[39] Qingyu Ma and Bin He. Investigation on magnetoacoustic signal generation with magnetic induction and its application to electrical conductivity reconstruction. *Physics in medicine and biology*, 52(16):5085, 2007.

[40] Jennifer L Mueller and Samuli Siltanen. *Linear and nonlinear inverse problems with practical applications*, volume 10. Siam, 2012.

[41] Jennifer L Mueller, Samuli Siltanen, and David Isaacson. A direct reconstruction algorithm for electrical impedance tomography. *Medical Imaging, IEEE Transactions on*, 21(6):555–559, 2002.

[42] Adrian I Nachman. Reconstructions from boundary measurements. *Annals of Mathematics*, pages 531–576, 1988.

[43] Adrian I Nachman. Global uniqueness for a two-dimensional inverse boundary value problem. *Annals of Mathematics*, pages 71–96, 1996.

[44] F. Natterer. Attenuation correction in emission tomography. In *Inverse problems: an interdisciplinary study (Montpellier, 1986)*, Adv. Electron. Electron Phys., Suppl. 19, pages 21–33. Academic Press, London, 1987.

[45] F. Natterer and H. Herzog. Attenuation correction in positron emission tomography. *Math. Methods Appl. Sci.*, 15(5):321–330, 1992.

[46] Frank Natterer and Frank Wübbeling. *Mathematical methods in image reconstruction*, volume 5. Siam, 2001.

[47] Lassi Päivärinta, Alexander Panchenko, and Gunther Uhlmann. Complex geometrical optics solutions for Lipschitz conductivities. *Revista Matematica Iberoamericana*, 19(1):57–72, 2003.

[48] Benjamin Palacios, Gunther Uhlmann, and Yiran Wang. Quantitative analysis of metal artifacts in X-ray tomography. *arXiv preprint arXiv:1712.01974*, 2017.

[49] Bent Petersen. *Introduction to the Fourier transform & pseudo-differential operators*. Pitman Advanced Publishing Program, 1983.

[50] Jerry L Prince and Jonathan M Links. *Medical imaging signals and systems*. Pearson Prentice Hall Upper Saddle River, New Jersey, 2006.

[51] Lingyun Qiu and Fadil Santosa. Analysis of the magnetoacoustic tomography with magnetic induction. *SIAM Journal on Imaging Sciences*, 8(3):2070–2086, 2015.

[52] Eric Todd Quinto. Singularities of the X-ray transform and limited data tomography in $\mathbf{R}^2$ and $\mathbf{R}^3$. *SIAM J. Math. Anal.*, 24(5):1215–1225, 1993.

[53] Johann Radon. *Theorie und anwendungen der absolut additiven mengenfunktionen*. Hölder, 1913.

[54] Alexander Ramm and Alexander Zaslavsky. Reconstructing singularities of a function from its Radon transform. *Mathematical and computer modelling*, 18(1):109–138, 1993.

[55] Mikko Salo. Inverse problems on Riemannian manifolds. University Lecture, 2010.

[56] Lawrence A Shepp and Yehuda Vardi. Maximum likelihood reconstruction for emission tomography. *IEEE transactions on medical imaging*, 1(2):113–122, 1982.

[57] Samuli Siltanen, Jennifer Mueller, and David Isaacson. An implementation of the reconstruction algorithm of A. Nachman for the 2d inverse conductivity problem. *Inverse Problems*, 16(3):681, 2000.

[58] Plamen Stefanov. The identification problem for the attenuated X-ray transform. *Amer. J. Math.*, 136(5):1215–1247, 2014.

[59] Plamen Stefanov and Gunther Uhlmann. Thermoacoustic tomography with variable sound speed. *Inverse Problems*, 25(7):075011, 2009.

[60] Ziqi Sun and Gunther Uhlmann. Generic uniqueness for an inverse boundary value problem. *Duke Math. J*, 62(1):131–155, 1991.

[61] Ziqi Sun and Gunther Uhlmann. Anisotropic inverse problems in two dimensions. *Inverse Problems*, 19(5):1001, 2003.

[62] John Sylvester. An anisotropic inverse boundary value problem. *Communications on Pure and Applied Mathematics*, 43(2):201–232, 1990.

[63] John Sylvester and Gunther Uhlmann. A uniqueness theorem for an inverse boundary value problem in electrical prospection. *Communications on Pure and Applied Mathematics*, 39(1):91–112, 1986.

[64] John Sylvester and Gunther Uhlmann. A global uniqueness theorem for an inverse boundary value problem. *Annals of mathematics*, pages 153–169, 1987.

[65] John Sylvester and Gunther Uhlmann. Inverse boundary value problems at the boundarycontinuous dependence. *Communications on pure and applied mathematics*, 41(2):197–219, 1988.

[66] John Sylvester and Gunther Uhlmann. Inverse problems in anisotropic media. *Contemp. Math*, 122(1):105–117, 1991.

[67] Shan Tong, Adam M Alessio, and Paul E Kinahan. Image reconstruction for PET/CT scanners: past achievements and future challenges. *Imaging in medicine*, 2(5):529, 2010.

[68] Gunther Uhlmann. *Inside out: inverse problems and applications*, volume 47. Cambridge University Press, 2003.

[69] Gunther Uhlmann. Electrical impedance tomography and Calderón's problem. *Inverse problems*, 25(12):123011, 2009.

[70] Gunther Uhlmann. Inverse problems: seeing the unseen. *Bulletin of Mathematical Sciences*, 4(2):209–279, 2014.

[71] Ilia Nestorovich Vekua. *Generalized Analytic Functions: International Series of Monographs on Pure and Applied Mathematics*, volume 25. Elsevier, 2014.

[72] A Welch, C Campbell, R Clackdoyle, F Natterer, M Hudson, A Bromiley, P Mikecz, F Chillcot, M Dodd, P Hopwood, et al. Attenuation correction in PET using consistency information. *IEEE Transactions on Nuclear Science*, 45(6):3134–3141, 1998.